A model intercomparison analysis for controls on C accumulation in North American peatlands

Bailu Zhao[1], Qianlai Zhuang[1,2], Claire Treat[3], Steve Frolking[4]

1Department of Earth, Atmospheric, and Planetary Sciences, Purdue University, West Lafayette, IN 47907, USA

2Department of Agronomy, Purdue University, West Lafayette, IN 47907, USA

3 Alfred Wegener Institute Helmholtz Center for Polar and Marine Research, Telegrafenberg A45, 14473 Potsdam, Germany

4 Institute for the Study of Earth, Oceans, and Space; University of New Hampshire, Durham NH USA

Correspondence to: qzhuang@purdue.edu

Key points:

- Peatlands tend to be C sources or weaker C sinks when insufficient precipitation suppresses net N mineralization and NPP.
- Peatlands tend to be C sources or weaker C sinks when drier climate leads to increasing water table depth.
- Both C-N feedback and water table change are important factors influencing peatland C balance.

Abstract

Peatland biogeochemical processes have not been adequately represented in existing earth system models, which might have biased the quantification of Arctic carbon-climate feedbacks. We revise the Peatland Terrestrial Ecosystem Model (PTEM) by incorporating additional peatland biogeochemical processes. The revised PTEM is evaluated by comparing with Holocene Peatland Model (HPM) in simulating peat physical and biogeochemical dynamics in three North American peatlands: a permafrost-free fen site, a permafrost-free bog site and a permafrost bog site. Peatland carbon dynamics are simulated from peat initiation to 1990 and then to year 2300. Model responses to the changes in temperature and precipitation are analyzed to identify key processes affecting peatland carbon accumulation rates. We find that the net C balance is sensitive to water table depth and nutrient availability. Future simulations to year 2300 are conducted with both models under RCP 2.6, RCP 4.5, and RCP 8.5. PTEM predicts these peatlands to be C sources or weaker C sinks when insufficient precipitation suppresses soil moisture and thereby net N mineralization and NPP, while HPM predicts the same when drier climate leads to increasing water table depth. Our results highlight the importance of water balance and C-N feedback on peatland C dynamics. With a warmer climate, these peatlands could become a weaker C sink or a source under drier conditions, otherwise a larger C sink if wetter. Improved understanding to peatland processes can help future quantification of peatland C dynamics in the boreal and Arctic regions.

1. Introduction

Northern high latitude permafrost region contains 472-496 Pg C in the top 1m soil layer (Hugelius et al., 2014; Köchy et al., 2015), and northern peatlands contain 415±150 Pg C

(Nichols & Peteet, 2019; Turunen et al., 2002). Peatlands initiate when ecosystem productivity persistently exceeds decomposition under wet conditions (Jones & Yu, 2010). After the Last Glacial Maximum (LGM, 21 ka BP – 18 ka BP), the warming climate led to ice sheet and glacier retreat and exposed land that had been covered by ice (MacDonald et al., 2006), allowing peatland formation in large expanses of low-lying areas such as the West Siberian Lowlands and the Hudson Bay Lowlands. Many studies suggest a majority (90%) of existing peatlands initiated during 12 – 8 ka BP or 13 – 8ka BP, when climate was warmer and more land was free from ice (Gorham et al., 2007).

Although undisturbed peatlands are generally C sinks, anthropogenic disturbance and climate change may switch peatlands into C sources (Frolking et al., 2011). For example, northern permafrost non-growing season CO_2 emissions (respiration) will increase under warmer climate (Natali et al., 2019), and peatland growing-season CO_2 emission will enhance under water-table drawdown (Huang et al., 2021). Deepening water table is partially caused by warmer climate (Huang et al., 2021), and anthropogenic drainage can also contribute to this process. Drainage not only enhances CO_2 emission from peatlands, but also increases the C loss from wildfires (Qiu et al., 2021; Turetsky et al., 2011). In addition to CO_2 emission impacts, CH_4 emissions can also increase by different ratios as permafrost thaw exposes previously frozen soil to anaerobic or aerobic decomposition (O'Donnell et al., 2012; Turetsky et al., 2002). In particular, the southern part of the northern hemisphere permafrost region (discontinuous and sporadic permafrost) is most vulnerable to permafrost thaw, which could contribute significant amount of C loss (Hugelius et al., 2020; Treat, Jones, Alder, et al., 2021). Although productivity also can increase with warmer climate and longer growing seasons under favorable moisture and nutrient conditions, decomposition is expected to increase more and global peatlands are projected to be a weaker C sink by the end of 21st century (Gallego-Sala et al., 2018) and possibly a C source by 2300 (Loisel et al., 2021).

To quantify peatland C stock at site to regional level and predict the possible response to climate change, a few process-based models which couple the effect of temperature, precipitation, vegetation shift, permafrost, and other factors have been developed. For example, LPJ-GUESS (Lund-Potsdam-Jena General Ecosystem Simulator) has been used to simulate the C accumulation rate until 2100 (Chaudhary et al., 2017). LPJ-GUESS simulated dynamical water table position (WTP) and assumed plant functional type (PFT) shifts according to WTP. The Holocene Peatland Model (HPM) has been used to simulate the development of peatland and the response of peatland permafrost to climate change (Frolking et al., 2014; Treat, Jones, Alder, et al., 2021).

Recently, a peatland version of the Terrestrial Ecosystem Model was developed to simulate tropical and North American peatland C accumulation during Holocene at both site and regional levels (Wang, Zhuang, & Yu, 2016). However, PTEM has several limitations on describing peatland processes. First, different from LPJ and HPM, there are single aggregate pools for soil C and N and for vegetation C and N in PTEM (Figure 1). Therefore, the C and N distribution among different PFTs, and differences in the way each PFT responds to environmental conditions cannot be simulated. However, since different PFTs differ in terms of their productivity, nitrogen requirements and litter decomposition rates, PFT dynamics could be an important factor influencing peatland C balance (Kuhry & Vitt, 1996; Oberbauer & Oechel, 1989; Williams & Flanagan, 1996). Second, PTEM does not simulate peat thickness or physical properties such as bulk density, or soil organic C content across the peat profile. When simulating peat decomposition processes, the amount of soil C that takes part in soil aerobic and anaerobic decomposition is unknown. To address this issue, PTEM assumes the fractions of total soil C undergoing soil aerobic and anoxic decomposition are constant (Wang, Zhuang, Yu, et al., 2016). Third, PTEM cannot simulate a shift in peatland type, i.e. the switch between fen and bog. However, since many peatlands make this transition (Charman, 2002), and since fens usually have higher productivity and decomposition rates than bogs, ignoring this process could cause uncertainties in long-term C balance simulations. Finally, the soil thermal module (STM) in PTEM reads a constant initial soil profile as input every month, which makes the simulated soil temperature below around 1m depth very insensitive with surface temperature. As a result, PTEM tends to fail to capture active layer depth (ALD) dynamics in long-term simulations in northern peatlands.

To improve PTEM representation of peatlands ecosystems, here we further develop PTEM by 1) dividing the aggregated vegetation C and N pool into three plant functional type pools representing moss, herb and shrub; 2) adding peat thickness as a dynamic variable, in addition to peat C and N stocks; 3) adding functionality for a fen to bog transition process during peatland development; and 4) improving the calculation of the soil thermal profile. PTEM's PFT classes, algorithms for calculating peat thickness, and implementation of fen-bog transitions were partially derived from HPM (Frolking et al., 2010; Treat, Jones, Alder, et al., 2021). To evaluate the new PTEM, we use observational data of peat physics including their thermal and hydrological as well as carbon dynamics and conduct PTEM and HPM simulations at three sites including both fen and bog, permafrost and non-permafrost, to analyze model differences. We test the capability of the revised PTEM to describe peatland dynamics and compare PTEM simulations with HPM results through: 1) simulating the site-level dynamics of three different types of peatlands from peat initiation to 1990 with PTEM and HPM; 2) testing the sensitivity of PTEM to temperature and precipitation and key parameters; 3) finding key variables controlling NPP and decomposition in both models, which are the two drivers controlling net peat accumulation and therefore net C exchange; 4) simulating peatland dynamics with both models at the three sites under multiple RCPs until 2300, and analyzing the mechanisms that cause differences in future projections.

2. Methods

2.1. Overview

In the methods section, we first introduce the study sites and observational data that are used for the site-level simulation. Second, a brief introduction to HPM is provided. Third, we describe the PTEM revisions in terms of plant functional types, peat accumulation and decomposition, fen to bog transition and soil thermal dynamics. Fourth, we introduce the model input data. Finally, we introduce the methods used to evaluate PTEM at the site level in terms of climate inputs and key parameter sensitivity, key controls of C balance and future simulation.

2.2. Study sites and observational data

Three sites with different peatland types, continuous core profiles and sufficient C data were chosen for evaluation of PTEM and comparison with HPM: Mariana Fen, about 300 km north of Edmonton, Alberta, Canada; Bear Bog near Cordova, AK USA; and Innoko Bog, about 150 km south of Koyukuk, AK, USA (Table 1). Mariana Fen vegetation is currently dominated by *Sphagnum angustifolium*, *Andromeda polifolia*, and *Scheuchzeria palustris* (Yu et al., 2014), and Innoko Bog vegetation is currently dominated by black spruce (*Picea mariana*) with the understory dominated by *Sphagnum fuscum* (Jones et al., 2017). Little vegetation information is available for the un-published Bear Bog site, but core data is available in the dataset compiled by Loisel et al. (2014), which suggests *Sphagnum* presence. The long-term mean temperature of Innoko Bog (-4.7°C) is lower than the other two sites (-0.2°C, -0.9°C), which results in permafrost at Innoko (Table 1). Permafrost was not found when peat cores were collected at Mariana Fen and Bear Bog. Bear Bog has 3-4 times more precipitation than the other two sites (Table 1). The reconstructed coarse-resolution TraCE 21ka dataset, which simulates monthly climate data from the Last Glacial Maximum to present using CCSM3 (He, 2011), shows that temperature and precipitation at the three sites have been stable since peat initiated (Appendix Figure 3).

2.3. The HPM model

HPM was designed specifically to simulate the interacting effects of peat profiles of temperature, moisture, anoxia, and litter quality on peat accumulation dynamics (Frolking et al., 2010). In HPM, peat profiles are tracked as annual cohorts, with each layer representing litter deposition in a year. In contrast to PTEM, HPM includes run-on/run-off processes based on total peat height, but does not simulate nitrogen dynamics. In each month, the NPP of each PFT is calculated independently and added up as the total NPP of the ecosystem. Each year the above ground annual NPP is converted into the uppermost peat deposition layer while below ground (root) NPP is deposited into shallow peat layers depending on rooting depth, and when permafrost exists, also depending on the depth of the top soil layer that thaws in summer and freezes in fall, i.e., active layer depth (ALD). HPM tracks mass loss of litter/peat, but does not disaggregate this into CO_2, CH_4, and DOC decomposition products. We use here the HPM-Arctic version of Treat, Jones, Alder, et al. (2021), which has a monthly time step, includes peat/soil freeze-thaw dynamics, active layer simulation, and limits vegetation to three PFTs – sedge, shrub, and moss.

2.4. PTEM revisions

This study revised PTEM to have a better representation of PFT dynamics, peat accumulation and decomposition, fen-bog transition and soil thermal dynamics (Figure 1). The major improvements include: a) the vegetation C and N pool is divided into three PFT C and N pools for moss, herb and shrub. The productivity of each PFT is a fraction of the ecosystem total productivity while the decomposition rate of the litter depends on the fraction of litter origin from each PFT; b) peat thickness is simulated, and the decomposition process depends on the position of the peat layer relative to the water table or frozen depth; c) a fen to bog transition is considered for peatlands when peat thickness exceeds a specified threshold, and PFT productivity and decomposition parameters change after a fen-bog transition; d) the soil thermal profile is initialized based on the long-term air temperature, and is updated in every month. Below we describe each of these improvements.

2.4.1. Plant Function Type dynamics

In PTEM, there are three peatland PFTs: mosses, herbaceous plants and shrubs. We assume that variation in each PFT's relative productivity is primarily influenced by water table depth (WTD):

$$GPP_{wtd-hb} = \frac{c_{max-hb}}{1+\exp\left(-hb_a \times (wtd - wtd_{hbmin})\right)} - \frac{c_{max-hb}}{1+\exp\left(-hb_b \times (wtd - wtd_{hbmax})\right)} \quad (1)$$

$$GPP_{wtd-srb} = \frac{c_{max-srb}}{1+\exp\left(-srb_a \times (wtd - wtd_{srbmin})\right)} - \frac{c_{max-srb}}{1+\exp\left(-srb_b \times (wtd - wtd_{hbmax})\right)} \quad (2)$$

where GPP_{wtd-hb} and $GPP_{wtd-srb}$ are the gross primary production (GPP) of herbaceous plants and shrub if only influenced by WTD. c_{max-hb} and $c_{max-srb}$ are the maximum C assimilated by herb and shrub (g C·m^{-2}·mon^{-1}). hb_a, hb_b, srb_a, srb_b are the fitting parameters describing the increase and decrease of GPP with WTD of herbaceous plants and shrub, respectively. wtd_{hbmin} and wtd_{srbmin} are the minimum WTD that allows herb and shrub to grow, while wtd_{hbmax} and wtd_{hbmax} are the maximum WTD that allows herb and shrub to grow. Different from herb and shrub, the dominance of moss is affected by both WTD and the abundance of vascular plants (i.e., shading).

$$GPP_{wtd-moss} = \frac{c'_{max-moss}}{1+\exp\left(-moss_a \times (wtd - wtd_{mossmin})\right)} - \frac{c'_{max-moss}}{1+\exp\left(-moss_b \times (wtd - wtd_{mossmax})\right)} \quad (3)$$

$$c'_{max-moss} = c_{max-moss} \times (1 + vas\_effect \times vas\_cover) \quad (4)$$

$$vas\_cover = \frac{GPP_{wtd-hb} + GPP_{wtd-srb}}{c_{max-hb} + c_{max-srb}} \quad (5)$$

where $GPP_{wtd-moss}$ is the GPP of moss if only influenced by WTD and the presence of vascular plants. $c'_{max-moss}$ is the maximum C assimilated by moss under the effect of vascular plants (g C·m^{-2}·mon^{-1}). $moss_a$ and $moss_b$, are the fitting parameters describing the increase and decrease of moss GPP with WTD. $wtd_{mossmin}$ and $wtd_{mossmax}$ are the minimum and maximum WTD that allows herb and moss to grow. $c_{max-moss}$ is the maximum C assimilated by moss if not affected by vascular plants (g C·m^{-2}·mon^{-1}), vas_effect is the effect of vascular plants on moss productivity, and vas_cover is the dominance of vascular plants.

As described in Raich et al. (1991), McGuire et al. (1992) and Zhuang et al. (2002), in PTEM, total gross primary production (GPP_{total}) is defined as:

$$GPP_{total} = c_{max} f(PAR) f(Phenology) f(Foliage) f(T) f(C_a, G_v) f(N) \quad (6)$$

where c_{max} is the maximum C assimilation rate of the entire ecosystem (g C·m^{-2}·mon^{-1}), $f(PAR)$ is the effect of photosynthesis active radiation, $f(Phenology)$ is the effect of monthly leaf area, $f(Phenology)$ is the effect of lead biomass, $f(T)$ is the effect of temperature,

$f(C_a, G_v)$ is the effect of CO_2 concentration and relative canopy conductance, and $f(N)$ is the effect of nitrogen availability. However, the GPP calculated in equation (6) does not describe the effect of water table on the dominance of PFTs. Therefore, GPP_{total} is distributed into each PFT by their theoretical GPP if only influenced by water table (i.e., the GPP calculated by equation (1-3)):

$$GPP_{pft} = \frac{GPP_{wtd-pft}}{GPP_{wtd-moss}+GPP_{wtd-hb}+GPP_{wtd-srb}} \times GPP_{total} \quad (7)$$

In the original version, PTEM calculates the litter fall C, maintenance respiration, growth respiration and net primary production (NPP) of the entire ecosystem. After adding PFTs, the vegetation C pool is divided into moss C pool, herb C pool and shrub C pool and the monthly growth in partitioned into each pool (Figure 1). The C fluxes into each pool are calculated separately for each PFT, but the algorithms remain the same as described in Raich et al. (1991). Similarly, the vegetation N pool is also further divided into moss, herb and shrub N pools, and the fluxes into and out of each pool (e.g. litter fall N, vegetation N uptake, N mobilization by vegetation and N resorption by vegetation) are calculated separately. These algorithms are well documented by McGuire et al. (1992) and Raich et al. (1991) remain the same in this study.

2.4.2. Peat accumulation and peat decomposition

The peat accumulation process in PTEM is now similar to HPM, with peat being vertically divided into multiple layers. In each month, the litter input is added to the top layer while decomposition is calculated for all the layers. When total peat thickness is less than 5cm, each layer is the peat deposition in one month. When the total peat thickness first exceeds 5cm, the monthly layers are aggregated into 1cm layers except for the top layer. Thereafter, for computational efficiency, peat thickness dynamics will be based on these 1cm layers, instead of monthly layers. In each month, litter is added to the top layer while the other layers become thinner as peat decomposes. Since the thickness of the layers are no longer 1cm, the peat profile will be re-interpolated into 1cm layers each month. The total thickness of peat is calculated by:

$$TotThick_i = \sum_0^i Thick_i \quad (8)$$

where *i* represents the number of layers, and $Thick_i$ is the thickness of layer *i* (cm). For each layer, $Thick_i$ is given by:

$$Thick_i = \frac{soilC_i}{densC_i \times 10000} \quad (9)$$

where $soilC_i$ is the soil organic C in layer *i* (g C·m^{-2}), $densC_i$ is the C density in layer *i* (g C·cm^{-3}), and 10000 is a unit-correction scalar. $densC_i$ is calculated by:

$$densC_i = dens_i \times C_{con} \quad (10)$$

where $dens_i$ is the bulk density of layer *i* (g·cm^{-3}) and C_{con} is the carbon content of the peat (0-1). $soilC_i$ is given by:

$$soilC_i = soilC_i' - R_{Hi} - CH_{4i} \quad (11)$$

where $soilC_i'$ is the soil organic C in the last month in layer i (g C·m^{-2}), R_{Hi} is the aerobic heterotrophic respiration (R_H) of layer i (g C·m^{-2}), and CH_{4i} is the anoxic decomposition (presented as methane production) of layer i (g C·m^{-2}). In PTEM, CH_4 production is a function of NPP, soil temperate, pH and redox potential effects on methanogenesis; the details of these algorithms are provided by Zhuang et al. (2004). We assume that methane production only happens in the layers below the water table and above the frozen depth if permafrost is present or the bottom of the peat if there is no permafrost. However, we assume R_H happens in both unsaturated and saturated layers, but not in frozen layers:

$$R_{Hi} = k_{di} soilC_i f(M_V) Q_{10i} m_i \tag{12}$$

where k_{di} is the R_H at 0°C for layer i (g C·m^{-2}), $f(M_V)$is the impact of soil moisture (M_V) on R_H, Q_{10i} is the soil temperature effect on R_H, and m_i is the fraction of remaining litter in layer i. $f(M_V)$ is described as:

$$f(M_V)_{unsat} = \begin{cases} \frac{1}{1+\exp(moista \times M_V + moistb)} & (M_V \leq 0.6) \\ exp(moistc \times M_V + moistd) + moist_{min} & (M_V > 0.6) \end{cases} \tag{13}$$

$$f(M_V)_{sat} = moist_{\min-sat} + (f(M_V)_{unsat} - moist_{\min-sat}) \times \exp\left(-\frac{dbw_i}{moiste}\right) \tag{14}$$

$$M_V = \frac{VSM_{unsat}}{VSM_{sat}} \tag{15}$$

$f(M_V)_{unsat}$ is applied for peat layers above the water table. We use the same value for all the unsaturated layers. $moista$, $moistb$, $moistc$, $moistd$ are fitting parameters, while $moist_{min}$ is the effect of soil moisture on R_H under minimum moisture condition. VSM_{unsat} is the volumetric soil moisture of the unsaturated layer (m^3/m^3) and VSM_{sat} is the volumetric soil moisture of the saturated layer (m^3/m^3). $f(M_V)_{sat}$ is applied to the layers below the water table. We assume that below the water table, R_H still happens at a quite slow rate, which decreases with depth the layer below the water table. $moist_{\min-sat}$ is the minimum impact of soil moisture on R_H, dbw_i is the distance of layer i below the water table and $moiste$ is the fitting parameter.

$$Q_{10i} = RHQ10^{tempi/10} \tag{16}$$

where Q_{10i} is the effect of temperature on R_H in layer i, $RHQ10$ is the change in R_H due to 10°C temperature change and $tempi$ is the soil temperature of layer i (°C).

Peat bulk density increases with degree of decomposition, and is calculated as a function of fraction of remaining litter (m_i):

$$dens_i = dens_{min} + \frac{dens_{delta}}{1+\exp(densa \times m_i + densb)} \tag{17}$$

where $dens_{min}$ is the minimum bulk density (g·cm^{-3}), $dens_{delta}$ is the difference between the minimum and maximum bulk density (g·cm^{-3}), $densa$ and $densb$ are fitting parameter. m_i is calculated by:

$$m_i = \frac{soilC_i}{litterC_i} \quad (18)$$

where $litterC_i$ is the original litter input (g C·m^{-2}) of layer *i*. In each month, the litter C is a fraction of vegetation C of each PFT and the season of the year.

$$mon\_litterC_{pft} = \begin{cases} vegC_{pft} \times cfall_{pft} & first\ to\ second\ last\ month\ of\ the\ growing\ season \\ vegC_{pft} \times cfall_{fin-pft} & last\ month\ of\ the\ growing\ season \\ 0 & non-growing\ season \end{cases} \quad (19)$$

$$mon\_litterC_{total} = \sum_{pft=1}^{3} mon\_litterC_{pft} \quad (20)$$

where $mon\_litterC_{pft}$ is the monthly litter C falling from individual PFT (g C·m^{-2} mon^{-1}), $vegC_{pft}$ is the vegetation C of each PFT (g C·m^{-2}), $cfall_{pft}$ is the fraction of vegetation C that falls as litter for each PFT (0-1) during the first to the second last month of the growing season, $cfall_{pft-fin}$ is the fraction of vegetation C fall as litter for individual PFT (0-1) in the last month of the growing season, $mon\_litterC_{total}$ is the total monthly litter C of three PFTs (g C·m^{-2} mon^{-1}), and is the monthly C input to the peat. The growing season is defined as the months when the soil is not totally frozen. In case of no permafrost, litter fall happens in December.

2.4.3. Fen-bog transition

The PTEM simulated fen-bog transition can occur when the peat thickness exceeds a site-specific threshold (Frolking et al., 2010), which is usually estimated from the core profiles. If a peatland shifts from fen to bog, both its productivity and the decomposition rate of new litter decrease. This is at least in part, because in fens, nutrients come from both ground water and precipitation, while in bogs, nutrients only come from precipitation. Therefore, the change of water inflow could be an important factor of fen-bog transition. However, since PTEM does not include a run-on process, and a field record of run-on is not available for any of the study sites, the decline of productivity as fen switches to bog is simplified in PTEM to multiplying the maximum productivity by a scalar:

$$c_{max-bog} = c_{max-fen} \times scalar_{cmax} \quad (21)$$

where $c_{max-bog}$ is the maximum C assimilation rate of bogs (g C·m^{-2}·mon^{-1}), $c_{max-fen}$ is the maximum C assimilation rate of fens (g C·m^{-2}·mon^{-1}), and $scalar_{cmax}$ is a multiplier on 0-1 scale. Notably, the $c_{max-bog}$ and $c_{max-fen}$ are used to calculate GPP_{total}. The maximum C assimilation rate of individual PFTs (i.e. $c_{max-moss}$, c_{max-hb} and $c_{max-srb}$) are primarily used to describe the productivity of PFTs in response to WTD and are not changed during fen-bog transition. However, the rate of decomposition for each PFT's litter decreases after transitioning into a bog:

$$k_{dbog-pft} = k_{dfen-pft} \times scalar_{kd-pft} \quad (22)$$

where $k_{dbog-pft}$ is the R_H at 0°C for litter from an individual PFT in a bog (g C·m^{-2} mon^{-1}), $k_{dfen-pft}$ is the R_H at 0°C for litter origin from individual PFT in a fen (g C·m^{-2} mon^{-1}), and $scaler_{kd-pft}$ is the multiplier specified for each PFT (0-1).

In addition to these changes, the pH value is also adjusted to a lower value (Appendix Table 2) after a fen transition into a bog, which influences the rate of CH_4 production (Zhuang et al., 2004). In a case of no fen-bog transition, the scalars in equation (21-22) would be 1.

2.4.4. Peat thermal dynamics

The soil thermal module (STM) in PTEM is derived from a one-dimensional heat flow model (Goodrich, 1978). However, this module requires an initial soil thermal profile input, which used to be a set of fixed parameters (Zhuang et al., 2001). In this study, we initialize the soil profile according to the local climate. If the long-term average surface temperature exceeds 0 °C, we initialize the thermal profile by assuming no permafrost existence, otherwise we assume permafrost exists. In addition, we assume the initial temperature at 10m depth is the same as long-term surface average temperature.

When initializing without permafrost:

$$T_j = T_{ave} + (D_j - 10) \times G \tag{23}$$

where T_j is the initial temperature of layer j (°C), T_{ave} is the long-term average surface temperature (°C), D_j is the depth of layer j (m) and G is the geothermal gradient (°C·m^{-1}). Notably, the layers in STM are not the layers in peat accumulation and decomposition calculation. In the current PTEM, the soil initial profile includes 25 layers, thin near the surface and getting thicker with depth, with the deepest 43.5m below surface. When initializing with permafrost:

$$T_j = \begin{cases} T_{j-1}/1.5 & D_j < ALD_{max} \\ -T_{j-1}/1.5 & D_j > ALD_{max} \; and \; D_{j-1} < ALD_{max} \\ D_j \times tempa + tempb & D_j > ALD_{max} \; and \; D_{j-1} > ALD_{max} \\ T_{ave} + (D_j - 10) \times G & D_j \geq 10 \end{cases} \tag{24}$$

$$tempa = \frac{T_{ave}}{10 - ALD_{max}} \tag{25}$$

$$tempb = -\frac{ALD_{max} \times T_{ave}}{10 - ALD_{max}} \tag{26}$$

where T_{j-1} is the temperature of the upper layer *j-1* (°C), ALD_{max} is the maximum active layer depth (ALD, in cm) of the current site, D_{j-1} is the depth of the upper layer *j-1* (m), $tempa$ is the thermal gradient between the maximum active layer depth and 10m (°C·m^{-1}), and $tempb$ is the intercept that makes sure the temperature at ALD_{max} is 0°C while the temperature at 10m is T_{ave} (°C). ALD_{max} is calculated by Stefan Model (Romanovsky & Osterkamp, 1997):

$$ALD_{max} = coef \times \sqrt{STI_{day}} \tag{27}$$

where $coef$ is the multiplier $coef$ estimated from calibration against field data collected from Zackenberg fen in Greenland (López-Blanco et al., 2017)(Appendix). STI_{day} is the surface thaw index, defined as the accumulative daily surface temperature that exceeds 0°C (°C·day). Since PTEM uses monthly temperature rather than daily temperature, in order to estimate the time when the monthly temperature exceeds 0°C, we approximate the annual temperature as a trigonometric function of maximum monthly temperature, minimum monthly temperature and annual average temperature:

$$T(mon) = -\cos\left(\frac{mon \times 30}{180} \times \pi\right) \times \frac{T_{max} - T_{min}}{2} + T_{an-ave} \quad (28)$$

where $T(mon)$ is the monthly temperature, mon is the month of the year, T_{max} is the maximum monthly temperature, T_{min} is the minimum monthly temperature and T_{an-ave} is the annual average temperature (all temperature in °C). This approximation depicts the dynamics of monthly temperature in Zackenberg fen with a R^2 of 0.861 (Appendix). According to this approximation, the month that the temperature first rises to 0°C (mon_1) and first drops to 0°C (mon_2) are:

$$mon_1 = \frac{6}{\pi} \times \arccos\left(\frac{2 \times T_{an-ave}}{T_{max} - T_{min}}\right) \quad (29)$$

$$mon_2 = 4 \times \pi - mon_1 \quad (30)$$

Therefore, the accumulative monthly surface temperature that exceeds 0°C (STI_{mon}) is:

$$STI_{mon} = \sum_{mon1}^{mon2} T(mon) \quad (31)$$

If we assume there are 31 days in a month, then:

$$STI_{day} = 31 \times STI_{mon} \quad (32)$$

In the original PTEM, in every month, the soil thermal profile is reset to the initial condition written in a parameter file. Although the surface soil temperature responses to the surface air temperature promptly, the deep soil temperature is primarily affected by being reset to this initial input every month, and hardly changes. This makes the simulated frozen depth quite similar every year, with little sensitivity to the surface temperature. This causes uncertainty in the ALD simulation and influences the peat C balance (Treat & Jones, 2018). To address this issue, we update the soil thermal profile every month and use it as the initial profile of the next month. The STM is then calibrated by the observation record of Zackenberg, Greenland fen ALD (López-Blanco et al., 2020)(Appendix Figure 2).

2.5. Model input data

PTEM requires monthly temperature, precipitation, cloudiness and vapor pressure as climate inputs while HPM requires monthly temperature and precipitation. These climate data are derived from the TraCE 21ka dataset (He, 2011). In this study, only the data between 15ka BP-1990 are used. The coarse-grid TraCE data are interpolated to 0.5°×0.5° grids with bilinear interpolation to match the resolution of PTEM. Since the TraCE dataset does not include vapor pressure, the vapor pressure used in PTEM is calculated by:

$$vp = rh \times 6.107 \times 10^{\frac{7.5 \times T}{237.7 + T}} \quad (33)$$

where vp is the vapor pressure (hPa), rh is the relative humidity in the TraCE dataset (0-1), T is the air temperature (°C). Thereafter, the monthly TraCE data are bias-corrected with CRU v4.03 data (Harris et al., 2014) for the overlapping time period of these two datasets (1900-1990). In particular, we calculate the January-December monthly average temperature, precipitation, cloudiness and vapor pressure of the two datasets, and use the difference of temperature, and the ratios of precipitation, cloudiness and vapor pressure as the bias. Then the TraCE monthly data are corrected by monthly biases.

In this study, in addition to paleo-simulations, a future simulation is also conducted for each site until 2300. From the many CMIP5-based future climate data products, in this study we selected the IPSL-CM5A-LR model results because: a) it provides the climate data for both historical (1850-2005) and future periods (2006-2300); b) it covers the future scenarios of RCP2.6, RCP4.5 and RCP8.5; and c) among 24 CMIP5 models, it has one of the highest agreements with CRU data in terms of annual and seasonal average temperature, as well as the warming trend during 1901-2005 in Eurasia (Miao et al., 2014). Among 17 CMIP5 models, it has one of the lowest biases in terms of North America summer temperature and precipitation during 1979-2005 (Sheffield et al., 2013). Similar to the TraCE dataset, the bias correction procedure is conducted for the future dataset to match the CRU scale. Therefore, the climate inputs for future simulations are composed of CRU-bias-corrected data from three datasets: TraCE dataset (15 ka BP-1990), IPSL-CM5A-LR historical dataset (1990-2005) and IPSL-CM5A-LR future dataset (2006-2300).

In addition to the climate inputs, PTEM also requires annual atmospheric CO_2 level as an input. The CO_2 concentration (ppm) during 15 ka BP-1990 is provided by TraCE dataset (He, 2011), and the CO_2 concentration for three future scenarios during 1990-2300 is provided by Meinshausen et al. (2011). Spatially-explicit data of soil texture (percentage of silt, clay and sand; FAO-Unesco (1974)) and elevation (Zhuang et al., 2002) were also used for PTEM.

2.6. Site-level comparisons

2.6.1 Model calibration

PTEM parameters related to model improvements presented above are provided in Appendix Table 2 (parameters that apply to all three sites), and Appendix Table 3 (parameters calibrated for each site). The calibration was conducted with PEST (v17.2 for Linux), and the maximum C assimilated by the ecosystem (C_{max}), R_H at 0°C for different PFTs (k_d), and the scalars of C_{max} and k_d when fens transition to bogs were calibrated by age-peat thickness profiles derived from the core data. In particular, in Bear Bog and Innoko Bog, the fens transitioned to bogs when the net C accumulation rate showed an obvious decrease. For each site, the simulation started in 15ka BP, but peat accumulation did not start until the site-specific basal date.

For HPM, the adjusted parameters include maximum annual NPP, exponential decay rate of litter, exponential decline with depth in catotelm decomposition, the scalar of maximum annual NPP at fen-bog transition, run-on and run-off (Appendix Table 4). Similar to PTEM, these HPM parameters were adjusted to best approach the calibration result of PTEM, and also based on the age-peat thickness profiles. For each site, the simulation started at the basal date and peat accumulation was computed.

2.6.2 Sensitivity analysis to parametrization

It's likely that the coarse temporal and spatial resolution of the TraCE 21ka dataset doesn't capture the climate at these sites, and TraCE 21 ka dateset shows discrepancies with other climate model simulations at the regional level (Zhu et al., 2019). In order to address the uncertainty of historical climate input in PTEM, a sensitivity test on temperature and precipitation was conducted for the three sites. In particular, we created five sets of long-term (15 ka BP - 1990) temperature inputs: original, ±0.5°C and ±1°C, and five sets of long-term precipitation inputs: original, ±10% and ±20%. These generated 25 different combinations of temperature and precipitation inputs. The response of NPP, decomposition, total C accumulation to temperature and precipitation changes were analyzed.

In addition to climate sensitivity, the sensitivity to the key parameters of PTEM was also examined. These parameters include the maximum productivity ($C_{max-fen}$) and the decomposition rate ($k_{d-fen-pft}$). The maximum productivity parameters are adjusted by ±2.5% and ±5% while the decomposition rate parameters are adjusted by ±5% and ±10%. These adjustments were large enough to have an impact on the results, but not so large that peat failed to accumulate.

Correlations between productivity and decomposition and other key variables were calculated using the 5 by 5 matrices generated by 25 climate sensitivity scenarios to check the key controls on NPP, decomposition and peat C accumulation in both models. In PTEM, correlations were calculated between WTD, ALD, net N mineralization and NPP and between WTD, ALD, NPP and decomposition. In HPM, correlations were calculated between WTD, ALD and NPP, decomposition.

2.6.3 Future scenarios

Finally, we also run HPM and PTEM simulations for the three future scenarios until 2300 and compare their C balance in response to projected climate change. Mechanisms behind the C balance dynamics are considered in terms of the key variables found in the last step. The different performances of the two models are analyzed and compared.

3. Results

3.1. Comparison of model output to peat core observations

The peat thickness and soil organic C have similar profiles with time as the peat core data (Figure 2), and simulated contemporary peat thickness and soil organic C agree with the observations (Table 2). The two models simulate similar rates of NPP and decomposition (Figure 2). The NPP and decomposition of both bogs drop when fen transitions to bog. As a perennial fen site, long-term NPP and decomposition of Mariana Fen are higher than Bear Bog and Innoko Bog, while the two bogs are similar.

The WTD simulated by HPM shows higher variability and is shallower than simulated by PTEM. Although the precipitation of Bear Bog is much higher than the other two sites (Table

1, Appendix Figure 3), its WTD is not shallower than the other two sites. For HPM, run-off balances out the precipitation. On the contrary, Mariana Fen is assumed to be very low net run-off as a fen site, and Innoko Bog is not thick enough to have high run-off (Appendix Figure 4). In PTEM, since the run-off related to peat thickness is not considered, the reason for the deep WTD of Bear site is the high AET balancing out the precipitation.

Although permafrost did not exist when the cores were collected from Mariana Fen and Bear Bog, both models indicate permafrost existence in the history of these two sites (Appendix Figure 5). HPM simulates fewer years with frozen soil existence than PTEM for Mariana Fen (HPM: 3451 years vs. PTEM: 7045 years), while, the average ALD for the years with permafrost shallower in HPM than in PTEM (HPM: 102 cm vs. PTEM: 184 cm). HPM also simulates fewer years with frozen soil existence than PTEM for Bear Bog (HPM: 35 years vs. PTEM: 1556 years), and shallower average ALD when permafrost exists (HPM: 83 cm vs. PTEM: 164 cm). However, for Innoko, the coldest site, HPM and PTEM do not have much difference in terms of years of frozen soil existence and average thaw depth (HPM: 6151 years vs. PTEM: 6137 years; HPM: 79 cm vs. PTEM: 76 cm) (Appendix Figure 5). Notably, at the year of core collection, both HPM and PTEM simulate no permafrost in Mariana Fen and Bear Bog, and both simulate permafrost existence in Innoko Bog (Appendix Figure 6), which agrees with the field record (Table 1).

3.2. Model uncertainty due to uncertain past climate

PTEM NPP and decomposition increase with temperature regardless of precipitation change (Figure 3). In particular, when temperature increases by 1°C and precipitation does not change, NPP increases by 6 g C m^{-2} yr^{-1} (4%), 10 g C m^{-2} yr^{-1} (16%) and 5 g C m^{-2} yr^{-1} (7%) for Mariana fen, Bear bog and Innoko bog, respectively (Figure 3 ((1-3)a)). For precipitation, NPP decreases with precipitation increase only in Bear Bog while the opposite trend is found for Mariana Fen and Innoko Bog. However, when the precipitation increases by 20% and temperature does not change, the changes of NPP in Mariana Fen and Innoko Bog are small (increases by 1 g C m^{-2} yr^{-1} and 0 g C m^{-2} yr^{-1}, 1% and 0% respectively), indicating NPP is not very sensitive to precipitation in these two sites. For the much wetter Bear Bog, NPP decreases by 7 g C m^{-2} yr^{-1} (11%) corresponding to 20% precipitation increases (Figure 3 (1-3)a).

Decomposition also increases with temperature at all three sites, regardless of precipitation change. In particular, when precipitation does not change and temperature increases by 1°C, decomposition increases by 10 g C m^{-2} yr^{-1} (9%), 8 g C m^{-2} yr^{-1} (17%) and 4 g C m^{-2} yr^{-1} (7%) respectively (Figure 3 ((1-3)b)). For Bear Bog and Innoko Bog, decomposition generally decreases with higher precipitation. When the precipitation increases by 20% and temperature does not change, decomposition decreases by 3 g C m^{-2} yr^{-1} (7%) and 1 g C m^{-2} yr^{-1} (1%, Figure 3 (2b) & (3b)). On the contrary, for Mariana Fen, decomposition generally increases with precipitation (Figure 3 (1b)). Notably, in PTEM, although decomposition responded to precipitation differently in three sites, it is essentially not sensitive to precipitation in Mariana Fen and Innoko Bog, with only minor difference observed along the precipitation axis (Figure 3 (1b)).

As the balance between NPP and decomposition, the soil C decreases in Mariana Fen as climate becomes warmer and drier, with the largest decrease of 53 kg C m^{-2} (17%) as temperature increases by 1°C and precipitation decreases by 20% (Figure 3 (1c)). On the contrary, the C accumulation at Bear Bog is higher under warmer and drier conditions, with 88 kg C m^{-2} (47%) more soil C under the +1°C and -20% precipitation combination (Figure 3 (2c)). Innoko Bog has the highest C accumulation rate under the warmer and wetter climate, with the largest decrease of 11 kg C m^{-2} (10%) as temperature increases by 1°C and precipitation increases by 20% (Figure 3 (3c)).

3.3. Model sensitivity to key PTEM parameters: Productivity and decomposition

3.3.1. Effects of Productivity and decomposition on Soil C stocks

The model sensitivity of PETM to the maximum productivity and rate of decomposition (C_{max} and $k_{d\text{-}pft}$) parameters, was tested for the three sites. Relative changes in peat soil organic C stock are used to represent relative changes in the long-term C balance (Table 3). For all three sites, the total soil organic C is more sensitive to the maximum productivity (3.7% - 5.2% in response to 1% parameter change) while less sensitive to the decomposition rates (-0.6% - -0.4% in response to 1% parameter change). Notably, when changes of organic soil C stock corresponding with 1% parameter changes are averaged, the standard deviations are relatively small. This indicates that although influenced by other parameters and site conditions, PTEM is almost linearly correlated with the maximum productivity and the decomposition rates in all three sites (Table 3).

3.3.2 Key controls on NPP

In PTEM, for all three sites, NPP significantly correlates with net N mineralization ($P<0.001$, Table 4). In Mariana Fen and Innoko Bog, NPP significantly correlates with WTD ($P<0.01$), but this correlation is not found in Bear Bog (Table 4). In all three sites, higher NPP significantly correlates with deeper ALD during years with permafrost present ($P<0.05$). The reason for this correlation is because temperature influences NPP, net N mineralization and ALD. Net N mineralization influences NPP such that higher mineralization rates correspond to higher nutrient availability and higher NPP. Although WTD significantly correlates with NPP, it is not a key control over NPP in these simulations because WTD varies within ±0.5 cm with all climate inputs in all three sites (Appendix Figure 7 2(a-c)). Furthermore, in Mariana Fen, WTD has a very weak correlation with net N mineralization (Table 4).

In HPM, NPP is significantly correlated with WTD in three sites ($P<0.001$), while significantly correlated with ALD only in Bear Bog (positively, $P<0.001$) and Innoko Bog (negatively, $P<0.05$). The correlation between NPP and WTD arises from HPM's simulation of NPP as a nonlinear function of WTD, with each PFT having a different optimum. In addition, NPP is also a function of ALD when permafrost is present, which results in the correlation between NPP and ALD in Innoko Bog. For Bear Bog where permafrost does not always exist, the correlation between NPP and ALD is more likely a result of the coupled correlation between NPP and temperature and between temperature and ALD.

3.3.3 Key Decomposition controls

Decomposition in PTEM is composed of soil aerobic respiration (R_H) and anaerobic decomposition (CH_4). In all three sites, R_H and CH_4 significantly correlate with ALD ($P<0.001$, Table 4). R_H correlates with ALD negatively because they are both influenced by soil temperature (R_H increases with warming and ALD becomes deeper or more negative). However, for CH_4, the correlation with ALD occurs because 1) temperature is influential to both ALD and CH_4; and 2) ALD determines the lower boundary of CH_4 production (Table 4). For Mariana Fen and Bear Bog, the patterns of decomposition variation are consistent with the patterns of NPP variation because the decomposition of these two sites relies more on anaerobic pathways (e.g. CH_4 production), which is a function of NPP. This is supported by the highly significant correlation between CH_4 production and NPP in all three sites ($P<0.001$, Table 4). For Innoko Bog, CH_4 production is much lower and the total decomposition is mainly due to R_H.

For HPM, a significant correlation is found between decomposition and WTD in all three sites. The correlation is based on two conditions of HPM: 1) both WTD and decomposition are functions of water filled pore space (WFPS); and 2) WTD determines the boundary of aerobic and anaerobic decomposition. The aerobic decomposition rate is higher than the anaerobic rate, so as WTD increases, decomposition tends to increase. Decomposition in Mariana Fen and Innoko Bog also significantly correlates with ALD, because 1) both decomposition and ALD are the functions of soil thermal profile; and 2) when ALD becomes deeper, more organic matter will be decomposing and decomposition rates will tend to increase (Table 4).

3.4. Future simulations

3.4.1. Changes in water table

In PTEM, since water run-on and run-off are not considered, the WTD is mainly determined by the balance between AET and precipitation (Table 4), while AET tends to increase with precipitation (Appendix Figure 7 1(a-c)). From RCP 2.6 to RCP 8.5, for Mariana Fen and Innoko Bog, precipitation only increases by 3-12 mm yr^{-1}, and AET shows almost no change (Table 5). With minor changes in both AET and precipitation, the changes in WTD are also minor (Table 5). On the contrast, for Bear Bog, from RCP 2.6 to RCP 8.5, precipitation increases by 13-77 mm yr^{-1} and AET increases by 5-30 mm yr^{-1} (Table 5). Since the increases in AET do not exceed the increases in precipitation, the WTD becomes shallower and the site wetter.

In HPM, in addition to AET and precipitation, run-on and run-off also influence the water balance (Table 5). For Mariana Fen and Innoko Bog, changes in run-on, run-off and precipitation are not as large as the increases in AET and their WTD becomes deeper. However, for Bear Bog, the total of run-off and AET increase is large enough to offset the increase in precipitation and the WTD change is small (<4cm) (Table 5).

3.4.2. Changes in net N mineralization

In PTEM, net N mineralization is partially influenced by decomposition rate and soil water content, which can be reflected by WTD (Table 4). For all three sites, with shallower

WTDs (i.e., higher soil moisture content) and higher decomposition rates, net N mineralization during 1990-2300 tends to be higher than that during 1950-1990 (Table 5). However, N mineralization only become substantially higher under RCP 8.5 at Bear Bog (increasing by 326 mg N m^{-2} yr^{-1}). For Mariana Fen and Innoko Bog, although climate warms and decomposition rate increases, with the slight change in soil moisture/WTD, net N mineralization does not always increase with temperature (Table 5).

3.4.3. Effects of permafrost degradation

At Mariana Fen and Innoko Bog, permafrost thaw is simulated by both models (Appendix Figure 10). In Mariana Fen, permafrost is essentially gone after the early 21 century under all RCP scenarios (Appendix Figure 10 (1-6)a) and the correlations between NPP, decomposition (includes R_H and CH_4 for PTEM) and ALD are generally not significant ($P>0.05$, Appendix Table 5).

For Innoko Bog, in PTEM, compared with RCP 2.6, ALD deepens under RCP 4.5 and RCP 8.5. In particular, from RCP 2.6 to RCP 4.5, an additional 12.7 cm of peat is thawed; from RCP 4.5 to RCP 8.5, permafrost totally degrades. In HPM, although the ALD under RCP 8.5 is 45 cm deeper than under RCP 4.5, ALD approaches the peat bottom under RCP 4.5 and only 2.1 cm of peat thaws on average (Appendix Figure 10 (2c) and (3c)). Given the thin peat layer that thaws during climate warming, the amount C released from permafrost peat is quite small, and has minor effect on the peat decomposition. Therefore, despite more C thaw in PTEM under RCP 4.5 and RCP 8.5 than under RCP 2.6, the peat is still a C sink, indicating the C losses from permafrost thaw do not override the positive effect of temperature on peat C accumulation.

3.4.4. Future C balance

Whether a site becomes a C sink or C source depends on the balance between NPP and decomposition. Warmer climate stimulates both processes, but the other factors may offset this effect. For all three sites, with little influence of permafrost thaw on decomposition, the C balance in PTEM is mainly driven by net N mineralization on NPP and in HPM driven by WTD on decomposition. For example, in PTEM, as climate becomes warmer, net N mineralization decreases and limits NPP in Mariana Fen, but the opposite trend is found in Bear Bog. Therefore, although Mariana Fen and Bear Bog are both C sinks under RCP 2.6 by 6 kg C m^{-2} and 22 kg C m^{-2}, Mariana Fen becomes a weak C source under RCP 4.5, and stronger C source of 43 kg C m^{-2} under RCP 8.5, while Bear Bog becomes a stronger C sink by 34 kg C m^{-2} and 64 kg C m^{-2} under RCP 4.5 and RCP 8.5 (Table 5). Innoko Bog, on the other hand, shows little variation in net N mineralization compared with Mariana Fen and Bear Bog. From RCP 4.5 to RCP 8.5, the temperature rises as much as Bear Bog, and WTD is almost unchanged, while the C sink only increases by 2 kg C m^{-2}. Compared with the C sink increase of 30 kg C m^{-2} at Bear Bog, it's reasonable to speculate the decrease in net N mineralization suppresses the C sink capability of Innoko Bog.

For HPM, all three sites are weak C sinks under RCP 2.6 (Mariana Fen: 7 kg C m^{-2}, Bear Bog ad Innoko Bog: 5 kg C m^{-2}, Table 5). For Mariana Fen and Innoko Bog, with the warmer climate and deepening WTD, more C is exposed to aerobic decomposition and the sites switch to

C sources under RCP 8.5 (Mariana Fen: 82 kg C m^{-2}, Innoko Bog: 6 kg C m^{-2}). On the contrary, for Bear Bog, with sufficient precipitation to stabilize WTD, the increases in NPP overrides the increase in decomposition and the site becomes stronger C sink under RCP 4.5 and RCP 8.5 by 8 kg C m^{-2} and 52 kg C m^{-2} respectively.

4. Discussion

4.1. Overview

In this section, we first compare our model simulation with literature to evaluate the efficacy of both models in capturing peatland C fluxes and stocks. Second, we discuss the major drivers of future C balance under current model framework, and emphasize the importance of precipitation. Third, we analyze the effect of model structure difference on future C projection and argue that run-on and run-off and C-N feedback are important processes in peatland models. Finally, we discuss the risk of permafrost degradation and analyze the reason that it does not have much impact on Innoko Bog. Notably, the ALD simulated in the discontinuous permafrost region by both models should be treated carefully.

4.2. Model performance in past simulations

Both models simulate the C fluxes and stocks of the three sites. As to stocks, the average C accumulation rate of three sites is 25.8 g C m^{-2} y^{-1} in PTEM and 24.9 g C m^{-2} y^{-1} in HPM. These values are ~10% larger than the northern peatland Holocene average of 22.9±2.0 g C m^{-2} y^{-1} reported by Loisel et al. (2014) and ~20% larger than the Canadian peatland Holocene average of 20.3 g C m^{-2} y^{-1} reported by Yu et al. (2009). However, they are close to 26.1 g C m^{-2} y^{-1} reported by Turunen et al. (2002). As to fluxes, no direct observations are available at these sites. Flux tower measurements in N-rich Zackenberg Fen in Greenland (74°28' N, 20°34' W) shows that NPP is 42-105 g C m^{-2} y^{-1} (López-Blanco et al., 2020; López-Blanco et al., 2017). Mariana Fen is warmer, and the simulation results with higher NPP (147-152 g C m^{-2} y^{-1}) seem reasonable. The bog simulations have lower NPP (64-65 g C m^{-2} y^{-1}) than the Mariana Fen simulations but still fall within the observation range at Zackenberg. In this study, the PTEM average CH_4 emissions in bogs are 12.1 g C m^{-2} y^{-1} and in poor fen is 21.3 g C m^{-2} y^{-1}, which are higher or approach the upper 95% confidence interval of bog (9.3 g C m^{-2} y^{-1}) and poor fen (21.7 g C m^{-2} y^{-1}) CH_4 emissions reported in Treat, Jones, Brosius, et al. (2021). Overall, both models simulate C fluxes and stocks with relatively high reliability.

4.3. Drivers of future C balance

The climate projection data used in this study is derived from IPSL-CMIP5-LR; its features are analyzed in Dufresne et al. (2013). IPSL-CMIP5-LR model predicts a global temperature change of 1.9K for RCP 2.6 and 12.7K for RCP 8.5, and the temperature change in North America is around 1.5 times the global average. This predicted temperature increase is higher than many other CMIP5 models (Palmer et al., 2018). Such rapid climate change could lead to unpredictable disruptions to ecosystems, including vegetation dynamics and disturbance not considered in the models.

Another feature of IPSL-CMIP5-LR model is that as temperature rises, part of northern North America shows precipitation increase and the rest almost no change. The sites studied had similar temperature increases, but the projected precipitation increase at Bear Bog is much higher than Mariana Fen and Innoko Bog (Table 5). A remote sensing-based study on cold and dry condition suggests that when water is limiting, the correlation between temperature and AET is negative (Sun et al., 2016). This trend is found in the PTEM simulation for Mariana Fen and Innoko Bog, which indicates that these two sites are water-limited (Appendix Figure 8 (2a) & (2c)). With water limit suppression of net N mineralization, Mariana Fen and Innoko Bog don't show as much NPP increase as Bear Bog (Figure 4).

For all three sites, for PTEM, decomposition increases as climate warms in both models (Figure 4). As the balance between NPP and decomposition, PTEM suggests Bear Bog to be a larger sink under warmer and wetter conditions, where sufficient precipitation and higher temperature increase NPP more than decomposition. The simulations for Mariana Fen and Innoko Bog project them to be a weaker sink or source under warmer and drier conditions, where the positive effect of temperature on NPP is offset by N deficiency (Appendix Figure 7 4(a-c), Figure 3 (1-3)a). In agreement with this study, a regional study on northern peatlands indicates that during 2100-2300, a drier climate will likely lead to lower soil C stock (Loisel et al., 2021). Similarly, another study indicates that drying peatlands will result in net emission increases of 0.86 Gt CO_2-eq yr^{-1} by the end of 21^{st} century (Huang et al., 2021). Therefore, the magnitude of precipitation increase will have a significant influence on the future C balance under warming climate.

4.4. The absence of run-on and run-off in PTEM

Given that the effects of precipitation, water availability, and water table are major controls on peatland C balance at these sites, it is important to consider model controls on water table position. One major difference between HPM and PTEM is that PTEM does not consider run-on from the peatlands surrounding watershed (significant for fens), nor base run-off. However, the future simulation of HPM indicates that run-on and run-off have a significant influence on the water balance, causing HPM to project quite different WTD compared with PTEM (Appendix Figure 9). If run-on and run-off were included in PTEM, the C balance in the future could be quite different for three reasons. First, run-on and run-off control peatland WTD significantly by the charging and discharging the peat (Glaser et al., 2016). For a fen site, although the net run-off could be low, run-on, whether from surface water inputs or groundwater recharge, plays an important role in maintaining the WTD, while for a bog site, run-on is generally negligible, but run-off can be more important than in fen sites (Weiss et al., 2006). For example, extensive drainage of peatlands enhances run-off but not run-on, thereby leading to deeper WTD, altering the plant and microbial community and influencing CH_4 emissions (Minkkinen et al., 2007). Second, run-on and run-off also influence nutrient availability in a peatland by delivering or removing nutrients (Limpens et al., 2006). Third, with different soil moisture levels, the net N mineralization rates are likely to be different and thereby influence NPP. In support of this idea, studies have shown that net N mineralization is significantly affected by soil moisture (Gao et al., 2016; Wang et al., 2006). Therefore, run-on and run-off are potential important variables to be added to PTEM, especially if peatland drainage or peatland fen-bog transition processes are to be modeled.

4.5. The influence of N availability

In addition to run-on and run-off, another major difference between HPM and PTEM is that PTEM explicitly considers the influence of N availability on productivity and decomposition. In PTEM, the available N for plants comes from N mineralization. Since NPP is sometimes suppressed by limited N mineralization in the future simulation (1990-2300, Appendix Figure 8), N is a limiting factor of productivity in all three sites. As N-limited ecosystems (Gunnarsson & Rydin, 2000), peatland productivity responds positively to N availability and nitrogen fertilization (Ojanen et al., 2019). Similarly, both this study and Bayley et al. (2005) find higher net N mineralization rates in fens than bogs (Appendix Figure 8), which partly explains the higher NPP at Mariana Fen during past simulations (Table 2). Therefore, it's important to consider N-NPP feedback processes in peatland models, and a different future C balance can be expected from HPM if these processes were added. In addition, field experiments in Canada and Western Europe and a modelling study all indicate that bogs and *Sphagnum* productivity are not very sensitive to, or could be depressed by, higher N availability, thereby increasing vascular plant coverage (Berendse et al., 2001; Granath et al., 2014; Gunnarsson & Rydin, 2000; Moore et al., 2019; Turunen et al., 2004). The feedback between N availability and vascular plant coverage is not included in PTEM, and may cause some uncertainties in the future C balance of the N-sufficient site (i.e. Bear Bog). While HPM is able to simulate vegetation shifts, the change is not triggered by N cycling but rather WTD and ALD.

As to decomposition, studies found that enhanced N availability promotes litter and peat decomposition (Bragazza et al., 2006; Ojanen et al., 2019; Song et al., 2018). For example, a study in Northeast China suggests that with increased N availability, some litter (e.g., litter from *E. vaginaturn and V. uliginosum*) shows enhanced decomposition (Song et al., 2018). Similarly, in an experiment in Finland, decomposition increased by 45% in fens under higher nutrient availability (Ojanen et al., 2019). An experiment in North America found strong correlation between CH_4 flux and N availability in both a patterned sedge fen and a raised Sphagnum bog (Updegraff et al., 2001). In agreement with these studies, PTEM aerobic decomposition rates are influenced by the C-N ratio of the input litter. However, this N-decomposition feedback is absent in HPM, except through litter quality differences between plant functional types. Missing N cycle may bias the future C balance estimate with HPM and any other peatland models that is lack of C and N feedbacks.

4.6. The influence of permafrost in future simulation

Many studies argue that permafrost thaw influences C balances at site and regional levels (Hugelius et al., 2020; O'Donnell et al., 2012; Schaefer et al., 2011). For example, a study in Alaskan arctic tundra (Plaza et al., 2019) measured 5.4% soil C loss per year as a result of permafrost degradation and lateral water outflow, while permafrost degradation account for less than half of the soil C loss. At the regional-scale, a modelling work indicates that as the ALD deepens, the northern permafrost region will switch from a C sink to a C source after 2100

(McGuire et al., 2018). Similarly, Hugelius et al. (2020) suggests the northern peatlands will become a C source as 0.8 to 1.9 million km^2 of permafrost thaws. However, in the simulations reported above, the effects of permafrost thaw on the site C balance are more varied. In particular, although both models simulate future permafrost degradation in Innoko Bog under RCP 4.5 and RCP 8.5 (Appendix Figure 10), the site does not become a C source in PTEM, and becomes a C source in HPM only under a very warm RCP 8.5 scenario (Figure 4) mainly because the WTD gets deeper, rather than permafrost degradation (Appendix Figure 9). In contrast to this study, a previous analysis of cores from Innoko bog shows that permafrost degradation caused the peatland to switch to a C source for about a century, then switch back to a C sink (Jones et al., 2017). A possible reason for this contradiction is that the cores used in Jones et al. (2017) are thicker and has more frozen peat C than the core used in this study. Since the simulated peat thickness in this study is close to the simulated ALD, the amount of peat C frozen in permafrost is relatively low. When permafrost thaws, the newly-thawed peat C remained saturated and cold and did not increase decomposition substantially (Elberling et al., 2013; Treat & Frolking, 2013). Anaerobic incubations of Innoko bog peat (Treat et al., 2014) suggest a CH_4 production rate is as low as 0.22 g C m^{-2} y^{-1} at -0.5°C, indicating that permafrost thaw does not increase anaerobic decomposition much for the newly-thawed, cold peat.

Notably, one common issue of both HPM and PTEM is that the simulated ALD of two adjacent years could differ significantly in the discontinuous permafrost region. For Mariana Fen, the ALD could differ by several meters in two adjacent years (Appendix Figure 6 & 10), which is too swift for permafrost (Lawrence et al., 2012). In the models, this is likely an artifact of the freeze-thaw algorithm, using an apparent heat capacity with a narrow temperature range (Marchenko et al. 2008), such that small temperature variations (~0.1°C) can switch the model designation between permafrost and active layer, while they may have little impact on carbon dynamics. However, for the warmer Bear Bog where permafrost rarely exists and the colder Innoko site where permafrost usually exists, this issue does not arise (Appendix Figure 6 & 10). Similar to this study, ALD estimation for sporadic permafrost zones tends to have the largest uncertainties (Beer et al., 2013; Dankers et al., 2011). Therefore, the simulated permafrost dynamics in this region should be interpreted with extra caution.

5. Conclusions

This study evaluates the revised PTEM with observations and HPM simulations at three northern peatland sites that are underlain with permafrost or permafrost free for the period 1990-2300. We find that main drivers to future C balance of these peatlands are different between two models. In particular, as climate becomes warmer, PTEM simulates the sites to be a C sink when precipitation is sufficient and net N mineralization is high enough to support productivity increases to override increased decomposition. HPM predicts that WTD dynamics are the major drivers to future C balance at these sites. Specifically, PTEM simulates that, with sufficient precipitation in Bear Bog, N remains sufficient and NPP overrides decomposition, making Bear Bog a stronger C sink from RCP 2.6 to RCP 8.5. On the contrary, Mariana Fen and Innoko Bog become warmer and drier, insufficient N availability suppresses NPP and thereby both sites switch to a weaker C sink (compared with Bear Bog) or a C source from RCP 2.6 to RCP 8.5.

We find the water run-on and run-off and C-N feedback are important processes to carbon dynamics in these peatlands, while both models are deficient in that because neither one includes both of these processes. Overall, the effect of permafrost on C dynamics is not significant at all three sites. We conclude that the future effort shall be directed to improving peatland thermal dynamics and peatland water run-on and run-off dynamics modeling and incorporating more adequate C-N feedbacks into current peatlands biogeochemistry models.

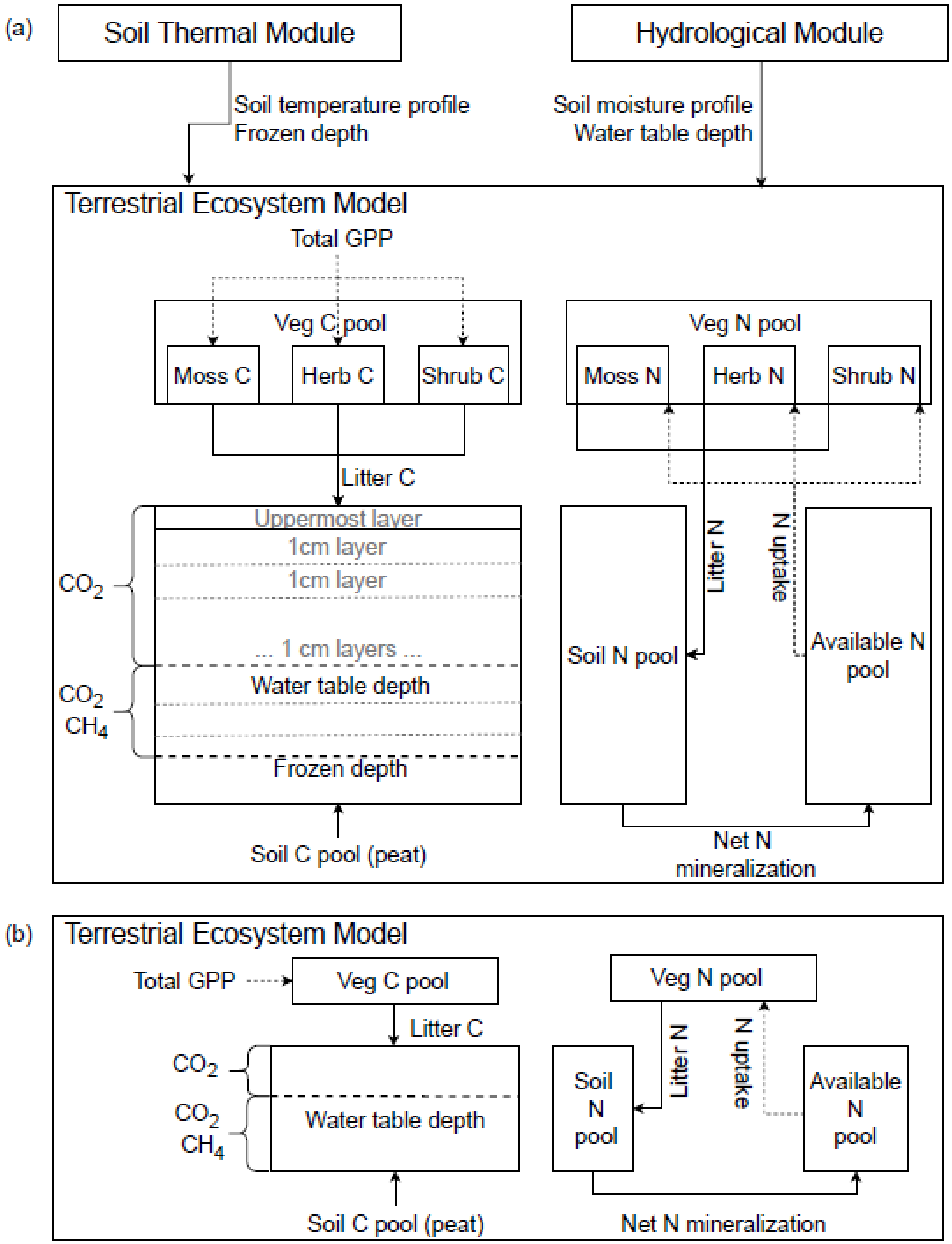

Figure 1. The structure of (a) the revised PTEM; and (b) the original Terrestrial Ecosystem Model.

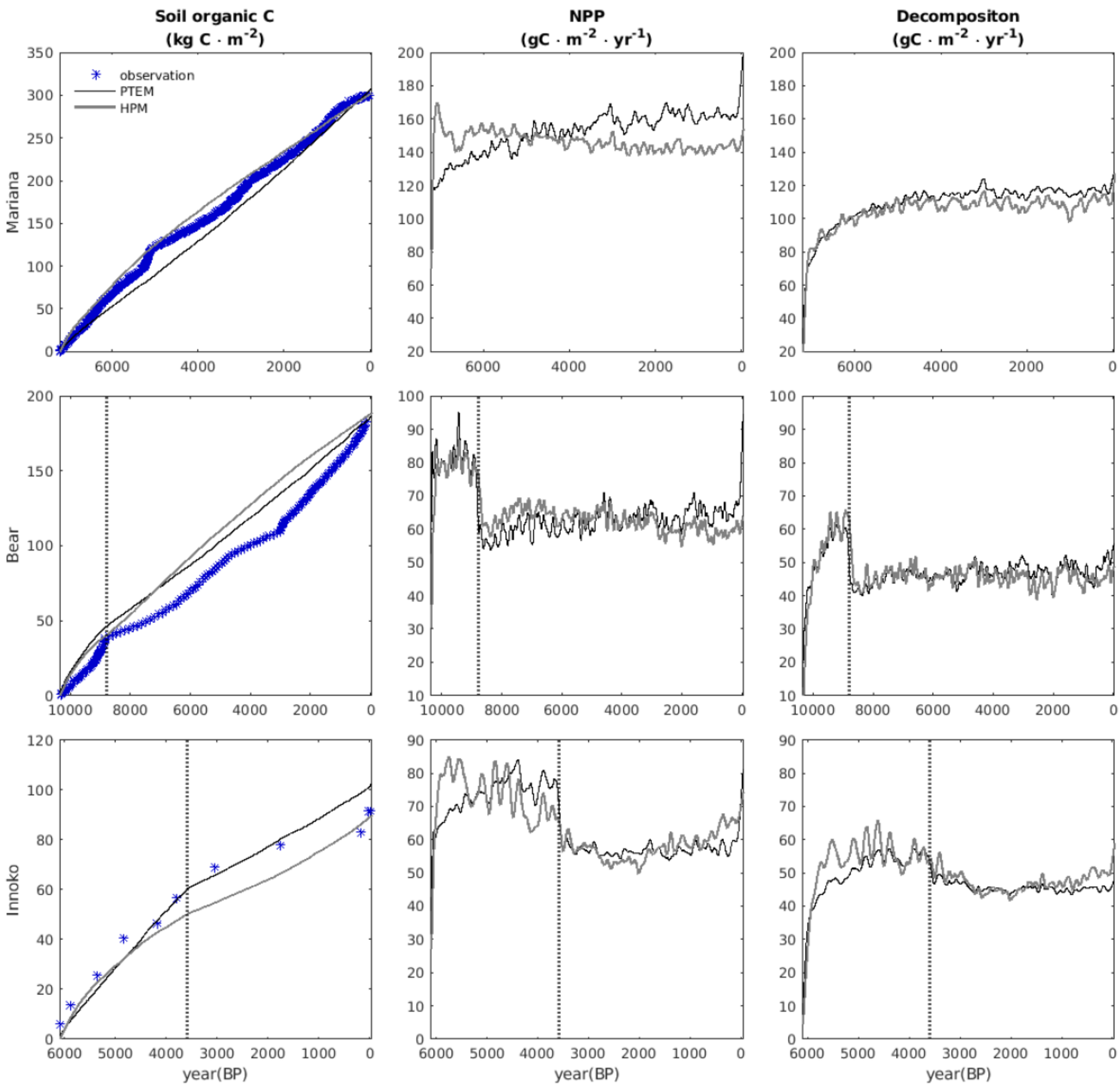

Figure 2. Simulated peat thickness, soil organic C, NPP and decomposition of HPM (light gray) and PTEM (dark gray) for three sites. The vertical line in Bear bog and Innoko bog panels show the time of fen to bog transition. The lines for NPP and decomposition are smoothed with the Matlab lowess function.

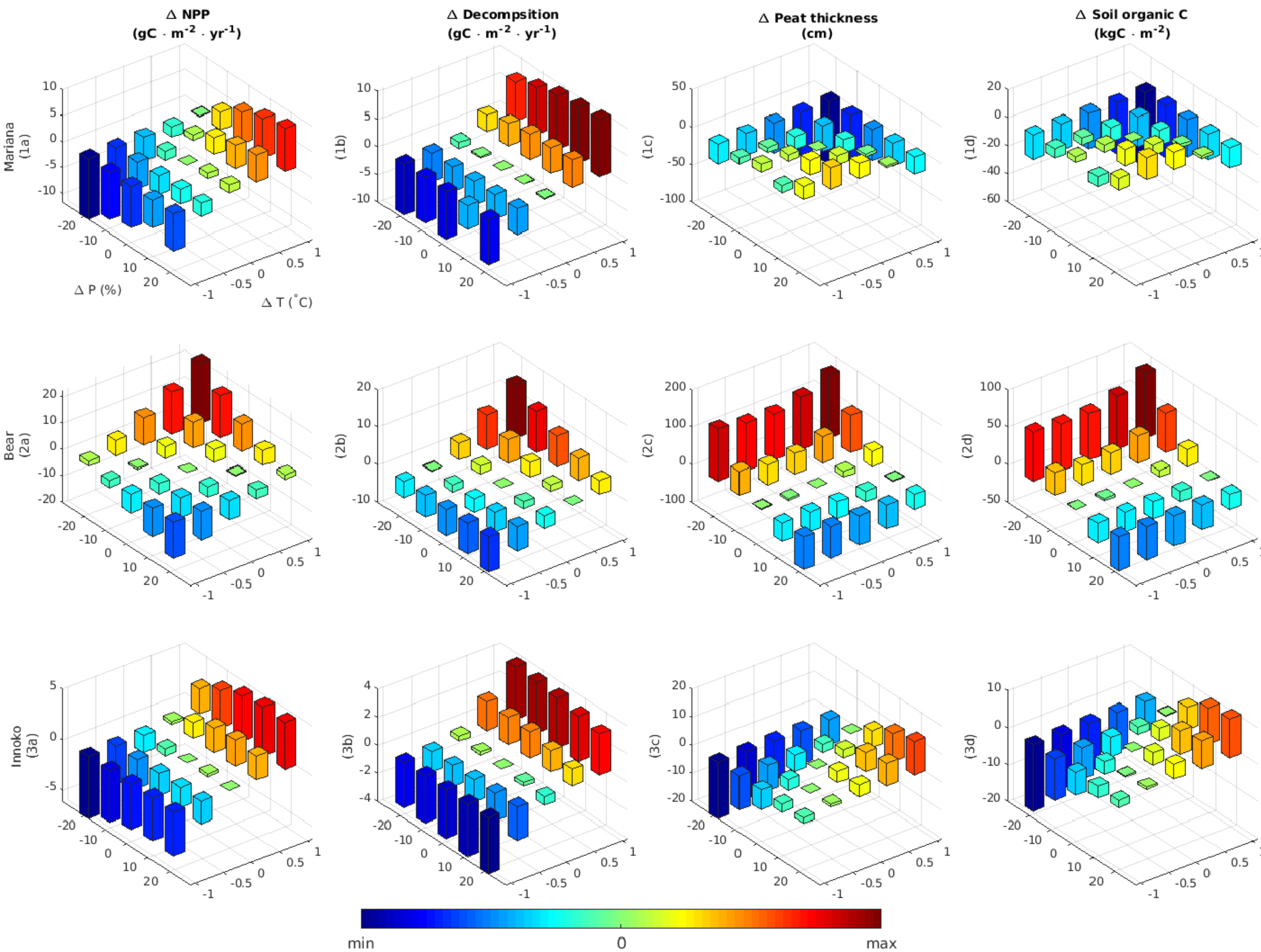

Figure 3. The sensitivity of long-term average annual NPP, decomposition, final peat thickness and total soil organic C in PTEM to changes in temperature and precipitation compared to the original forcing simulation. This factorial sensitivity analysis tested the response of C-related variables to temperature and precipitation change. Yellow-orange-red columns are >0, teal-blue columns are <0, green columns are ~0.

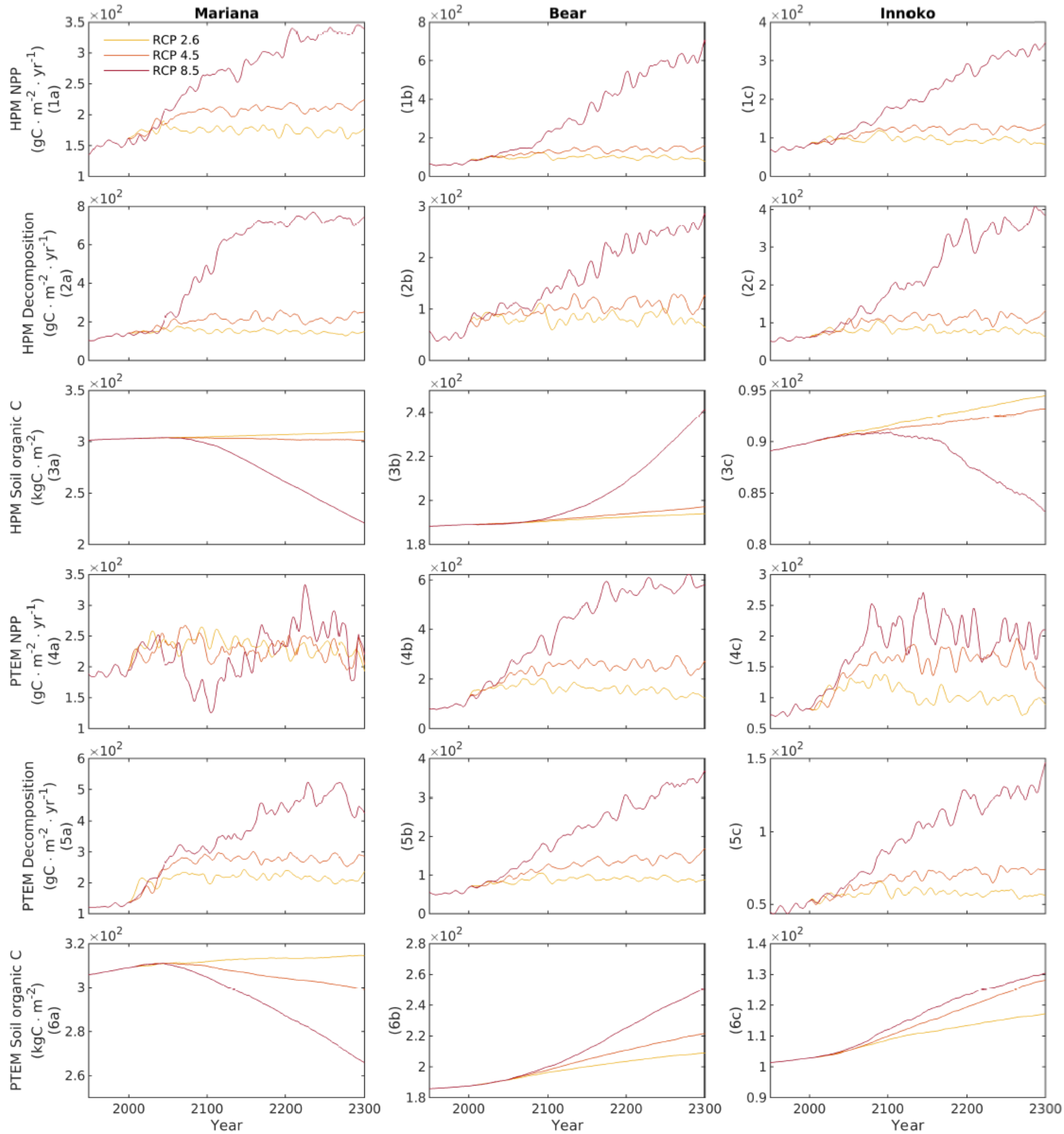

Figure 4. Under RCP 2.6, RCP 4.5 and RCP 8.5, the trends of NPP, decomposition and soil organic C at the three sites during 1950-2300 for both HPM (top three rows) and PTEM (bottom three rows). The lines of NPP and decomposition are smoothed with Matlab's Loess function.

Table 1. Site information

Site name	Core ID	Latitude, longitude	Basal age (BP)	Peatland type	Permafrost existence in coring year	Average annual temperature[*] (°C)	Average annual precipitation[*] (mm yr^{-1})	Coring year	Source
Mariana	Mariana_core MF03-1	55.9°N, 112.9°W	7222	Poor fen	N	-0.9	470	2003	Yu et al. (2014)
Bear	Bear_core1	60.5°N, 145.5°W	10357	Raised bog	N	-0.2	1560	2010	Unpublished[§]
Innoko	ODO-INN-UD1	63.6°N, 157.7°W	6100	Raised bog	Y	-4.7	360	2009	Jones et al. (2017)

[*] Average annual temperature and precipitation are calculated by the model forcing data for the period between basal age and 1990.

[§] The core for Bear bog was collected by Jonathan Nichols, and compiled in the database of Loisel et al. (2014).

Table 2. Simulated C-related variables of HPM and PTEM

Site name	Model	Final peat thickness (cm)	Total soil organic C (kg C m^{-2})	NPP (g C m^{-2} yr^{-1})	Decomposition (g C m^{-2} yr^{-1})
Mariana	Observed	471	300	--	--
	PTEM	466	309	152	110
	HPM	458	303	147	105
Bear	Observed	352	183	--	--
	PTEM	347	187	65	47
	HPM	340	189	65	47
Innoko	Observed	104	92	--	--
	PTEM	106	103	64	47
	HPM	104	90	64	50

* NPP and decomposition are averaged over basal date to 1990.

Table 3. Changes of PTEM organic soil C stock by 1990 resulting from parameter changes (%)

Parameter	Percentage change	Mariana	Bear	Innoko
Maximum productivity	-5.00	-18.0	-23.40	-17.51
(g C m^{-2} mon^{-1})	-2.50	-9.28	-12.60	-9.21
	2.50	9.37	13.02	10.66
	5.00	19.13	28.88	22.32
Relative change when parameter changes by 1%		3.72±0.09	5.18±0.46	3.98±0.46
Decomposition rate	-10.00	6.45	6.53	3.90
(g C m^{-2} mon^{-1})	-5.00	3.15	2.92	2.07
	5.00	-3.05	-3.05	-1.92
	10.00	-5.97	-5.89	-4.19
Relative change when parameter changes by 1%		-0.61±0.02	-0.61±0.03	-0.40±0.02

Table 4. Correlation coefficients and significance of correlation between the changes of variables in PTEM and HPM

	Mariana		Bear		Innoko	
	r	P	r	P	r	P
PTEM						
NPP-WTD	0.789	<0.001	-0.156	0.455	-0.598	0.002
NPP-ALD	-0.784	<0.001	-0.441	0.027	-0.962	<0.001
NPP-NETNMIN	0.752	<0.001	0.770	<0.001	0.852	<0.001
NETNMIN-WTD	0.222	0.287	0.457	0.022	-0.849	<0.001
NETNMIN-ALD	-0.852	<0.001	-0.798	<0.001	-0.932	<0.001
RH-WTD	0.048	0.818	0.114	0.588	-0.896	<0.001
RH-ALD	-0.828	<0.001	-0.642	<0.001	-0.975	<0.001
CH4-WTD	0.763	<0.001	0.187	0.371	-0.458	0.021
CH4-ALD	-0.762	<0.001	-0.635	<0.001	-0.909	<0.001
CH4-NPP	0.973	<0.001	0.935	<0.001	0.978	<0.001
WTD-AET	0.907	<0.001	0.991	<0.001	0.573	0.003
HPM						
NPP-WTD	-0.958	<0.001	-0.971	<0.001	-0.901	<0.001
NPP-ALD	0.094	0.654	0.754	<0.001	-0.487	0.014
Decomposition-WTD	-0.707	<0.001	-0.632	<0.001	-0.952	<0.001
Decomposition-ALD	-0.648	<0.001	0.171	0.415	-0.677	<0.001

Table 5. Differences between the values of key variables in HPM and PTEM

Site	Mariana			Bear			Innoko		
Scenario	RCP 2.6	RCP 4.5	RCP 8.5	RCP 2.6	RCP 4.5	RCP 8.5	RCP 2.6	RCP 4.5	RCP 8.5
Climate									
ΔTemperature (°C)	2	4	11	3	5	10	3	5	10
ΔPrecipitation (mm yr^{-1})	3	3	3	13	24	77	3	5	12
Average value differences during 1990-2300 and 1950-1990									
PTEM									
Water balance									
ΔAET (cm yr^{-1})	1	-4	-5	5	10	30	3	4	4
ΔWTD (cm)	0	0	2	1	1	4	-1	-1	1
C balance									
ΔNPP (g C m^{-2} yr^{-1})	40	37	31	70	144	333	28	72	110
ΔDecomposition (g C m^{-2} yr^{-1})	88	133	235	34	67	160	11	20	51
ΔR_H (g C m^{-2} yr^{-1})	11	19	74	8	14	34	8	13	31
ΔCH_4 (g C m^{-2} yr^{-1})	77	114	161	26	53	126	3	7	19
ΔNet N mineralization (mg N m^{-2} yr^{-1})	763	509	140	136	305	326	18	162	-25
ΔALD (cm)	1	-4	-5	-	-	-	-22	-42	-36
HPM									
ΔAET (cm yr^{-1})	6	12	22	7	13	40	6	10	20
ΔWTD (cm)	-1	-6	-19	-4	-4	-1	-3	-5	-8
ΔRun on (cm yr^{-1})	1	6	11	0	0	0	2	4	5
ΔRun off (cm yr^{-1})	-1	-3	-6	11	19	58	0	0	0
ΔNPP (g C m^{-2} yr^{-1})	22	50	117	37	66	279	23	44	139
ΔDecomposition (g C m^{-2} yr^{-1})	28	83	409	37	55	127	23	48	176
ΔALD (cm)	-33	-46	-25	-	-	-	-38	-276	-320
Total value differences between 2300 and 1990									
PTEM									
ΔPeat thickness (cm)	8	-22	-81	63	103	201	21	43	43
ΔSoil organic C (kg C m^{-2})	6	-9	-43	22	34	64	15	26	28
HPM									
ΔPeat thickness (cm)	5	-14	-141	7	14	137	5	3	-8
ΔSoil organic C (kg C m^{-2})	7	-1	-82	5	8	52	5	3	-6

* ALD values are used only when the soil is not totally thawed (when permafrost is present). Therefore, for Bear Bog, where permafrost does not occur during 1950-2300, there are no values.

References

Bayley, S. E., Thormann, M. N., & Szumigalski, A. R. (2005). Nitrogen mineralization and decomposition in western boreal bog and fen peat. *Écoscience, 12*(4), 455-465. Retrieved from https://doi.org/10.2980/i1195-6860-12-4-455.1. doi:10.2980/i1195-6860-12-4-455.1

Beer, C., Fedorov, A., & Torgovkin, Y. (2013). Permafrost temperature and active-layer thickness of yakutia with 0.5-degree spatial resolution for model evaluation. *Earth System Science Data, 5*. doi:10.5194/essd-5-305-2013

Berendse, F., Van Breemen, N., Rydin, H., Buttler, A., Heijmans, M., Hoosbeek, M. R., et al. (2001). Raised atmospheric co2 levels and increased n deposition cause shifts in plant species composition and production in sphagnum bogs. *Global Change Biology, 7*(5), 591-598. Retrieved from https://doi.org/10.1046/j.1365-2486.2001.00433.x. doi:https://doi.org/10.1046/j.1365-2486.2001.00433.x

Bragazza, L., Freeman, C., Jones, T., Rydin, H., Limpens, J., Fenner, N., et al. (2006). Atmospheric nitrogen deposition promotes carbon loss from peat bogs. *Proceedings of the National Academy of Sciences, 103*(51), 19386. Retrieved from http://www.pnas.org/content/103/51/19386.abstract. doi:10.1073/pnas.0606629104

Charman, D. (2002). *Peatlands and environmental change*. Chichester: John Wiley & Sons Ltd.

Chaudhary, N., Miller, P. A., & Smith, B. (2017). Modelling past, present and future peatland carbon accumulation across the pan-arctic region. *Biogeosciences, 14*(18), 4023-4044. Retrieved from https://www.biogeosciences.net/14/4023/2017/. doi:10.5194/bg-14-4023-2017

Dankers, R., Burke, E., & Price, J. (2011). Simulation of permafrost and seasonal thaw depth in the jules land surface scheme. *The Cryosphere Discussions, 5*, 1263-1309. doi:10.5194/tcd-5-1263-2011

Dufresne, J. L., Foujols, M. A., Denvil, S., Caubel, A., Marti, O., Aumont, O., et al. (2013). Climate change projections using the ipsl-cm5 earth system model: From cmip3 to cmip5. *Climate Dynamics, 40*(9), 2123-2165. Retrieved from https://doi.org/10.1007/s00382-012-1636-1. doi:10.1007/s00382-012-1636-1

Elberling, B., Michelsen, A., Schädel, C., Schuur, E. A. G., Christiansen, H. H., Berg, L., et al. (2013). Long-term co2 production following permafrost thaw. *Nature Climate Change, 3*(10), 890-894. Retrieved from https://doi.org/10.1038/nclimate1955. doi:10.1038/nclimate1955

FAO-Unesco. (1974). *Soil map of the world.* . Paris: Food and Agriculture Organization of the United Nations and the United Nations Educational, Scientific and Cultural Organization

Frolking, S., Roulet, N. T., Tuittila, E., Bubier, J. L., Quillet, A., Talbot, J., & Richard, P. J. H. (2010). A new model of holocene peatland net primary production, decomposition, water balance, and peat accumulation. *Earth Syst. Dynam., 1*(1), 1-21. Retrieved from https://www.earth-syst-dynam.net/1/1/2010/. doi:10.5194/esd-1-1-2010

Frolking, S., Talbot, J., Jones, M. C., Treat, C. C., Kauffman, J. B., Tuittila, E.-S., & Roulet, N. (2011). Peatlands in the earth's 21st century climate system. *Environmental Reviews, 19*(NA), 371-396. Retrieved from https://doi.org/10.1139/a11-014. doi:10.1139/a11-014

Frolking, S., Talbot, J., & Subin, Z. M. (2014). Exploring the relationship between peatland net carbon balance and apparent carbon accumulation rate at century to millennial time scales. *The Holocene, 24*(9), 1167-1173. Retrieved from https://doi.org/10.1177/0959683614538078. doi:10.1177/0959683614538078

Gallego-Sala, A. V., Charman, D. J., Brewer, S., Page, S. E., Prentice, I. C., Friedlingstein, P., et al. (2018). Latitudinal limits to the predicted increase of the peatland carbon sink with warming. *Nature Climate Change, 8*(10), 907-913. Retrieved from https://doi.org/10.1038/s41558-018-0271-1. doi:10.1038/s41558-018-0271-1

Gao, J., Feng, J., Zhang, X., Yu, F.-H., Xu, X., & Kuzyakov, Y. (2016). Drying-rewetting cycles alter carbon and nitrogen mineralization in litter-amended alpine wetland soil. *CATENA, 145*, 285-290. Retrieved from https://www.sciencedirect.com/science/article/pii/S0341816216302314. doi:https://doi.org/10.1016/j.catena.2016.06.026

Glaser, P. H., Siegel, D. I., Chanton, J. P., Reeve, A. S., Rosenberry, D. O., Corbett, J. E., et al. (2016). Climatic drivers for multidecadal shifts in solute transport and methane production zones within a large peat basin. *Global Biogeochemical Cycles, 30*(11), 1578-1598. Retrieved from http://pubs.er.usgs.gov/publication/70179639. doi:10.1002/2016GB005397

Goodrich, L. E. (1978). Efficient numerical technique for one-dimensional thermal problems with phase change. *International Journal of Heat and Mass Transfer, 21*(5), 615-621. Retrieved from https://www.sciencedirect.com/science/article/pii/0017931078900583. doi:https://doi.org/10.1016/0017-9310(78)90058-3

Gorham, E., Lehman, C., Dyke, A., Janssens, J., & Dyke, L. (2007). Temporal and spatial aspects of peatland initiation following deglaciation in north america. *Quaternary Science Reviews, 26*(3), 300-311. Retrieved from http://www.sciencedirect.com/science/article/pii/S0277379106002666. doi:https://doi.org/10.1016/j.quascirev.2006.08.008

Granath, G., Limpens, J., Posch, M., Mücher, S., & de Vries, W. (2014). Spatio-temporal trends of nitrogen deposition and climate effects on sphagnum productivity in european peatlands. *Environmental Pollution, 187*, 73-80. Retrieved from https://www.sciencedirect.com/science/article/pii/S0269749113006568. doi:https://doi.org/10.1016/j.envpol.2013.12.023

Gunnarsson, U., & Rydin, H. (2000). Nitrogen fertilization reduces sphagnum production in bog communities. *New Phytologist, 147*(3), 527-537. Retrieved from https://doi.org/10.1046/j.1469-8137.2000.00717.x. doi:https://doi.org/10.1046/j.1469-8137.2000.00717.x

Harris, I., Jones, P. D., Osborn, T. J., & Lister, D. H. (2014). Updated high-resolution grids of monthly climatic observations – the cru ts3.10 dataset. *International Journal of Climatology, 34*(3), 623-642. Retrieved from https://doi.org/10.1002/joc.3711. doi:https://doi.org/10.1002/joc.3711

He, F. (2011). *Simulating transient climate evolution of the last deglaciation with ccsm3.* (Doctor of Philosophy), UNIVERSITY OF WISCONSIN-MADISON, Madison, Wisconsin.

Huang, Y., Ciais, P., Luo, Y., Zhu, D., Wang, Y., Qiu, C., et al. (2021). Tradeoff of co2 and ch4 emissions from global peatlands under water-table drawdown. *Nature Climate Change, 11*(7), 618-622. Retrieved from https://doi.org/10.1038/s41558-021-01059-w. doi:10.1038/s41558-021-01059-w

Hugelius, G., Loisel, J., Chadburn, S., Jackson, R. B., Jones, M., MacDonald, G., et al. (2020). Large stocks of peatland carbon and nitrogen are vulnerable to permafrost thaw. *Proceedings of the National Academy of Sciences, 117*(34), 20438. Retrieved from http://www.pnas.org/content/117/34/20438.abstract. doi:10.1073/pnas.1916387117

Hugelius, G., Strauss, J., Zubrzycki, S., Harden, J. W., Schuur, E. A. G., Ping, C. L., et al. (2014). Estimated stocks of circumpolar permafrost carbon with quantified uncertainty ranges and identified data gaps. *Biogeosciences, 11*(23), 6573-6593. Retrieved from https://bg.copernicus.org/articles/11/6573/2014/. doi:10.5194/bg-11-6573-2014

Jones, M. C., Harden, J., O'Donnell, J., Manies, K., Jorgenson, T., Treat, C., & Ewing, S. (2017). Rapid carbon loss and slow recovery following permafrost thaw in boreal peatlands. *Global Change Biology, 23*(3), 1109-1127. Retrieved from https://doi.org/10.1111/gcb.13403. doi:https://doi.org/10.1111/gcb.13403

Jones, M. C., & Yu, Z. (2010). Rapid deglacial and early holocene expansion of peatlands in alaska. *Proceedings of the National Academy of Sciences, 107*(16), 7347. Retrieved from http://www.pnas.org/content/107/16/7347.abstract. doi:10.1073/pnas.0911387107

Köchy, M., Hiederer, R., & Freibauer, A. (2015). Global distribution of soil organic carbon – part 1: Masses and frequency distributions of soc stocks for the tropics, permafrost regions, wetlands, and the world. *SOIL, 1*(1), 351-365. Retrieved from https://soil.copernicus.org/articles/1/351/2015/. doi:10.5194/soil-1-351-2015

Kuhry, P., & Vitt, D. H. (1996). Fossil carbon/nitrogen ratios as a measure of peat decomposition. *Ecology, 77*(1), 271-275. Retrieved from https://doi.org/10.2307/2265676. doi:https://doi.org/10.2307/2265676

Lawrence, D. M., Slater, A. G., & Swenson, S. C. (2012). Simulation of present-day and future permafrost and seasonally frozen ground conditions in ccsm4. *Journal of Climate, 25*(7), 2207-2225. Retrieved from https://journals.ametsoc.org/view/journals/clim/25/7/jcli-d-11-00334.1.xml. doi:10.1175/JCLI-D-11-00334.1

Limpens, J., Heijmans, M. M. P. D., & Berendse, F. (2006). The nitrogen cycle in boreal peatlands. In R. K. Wieder & D. H. Vitt (Eds.), *Boreal peatland ecosystems* (pp. 195-230). Berlin, Heidelberg: Springer Berlin Heidelberg.

Loisel, J., Gallego-Sala, A. V., Amesbury, M. J., Magnan, G., Anshari, G., Beilman, D. W., et al. (2021). Expert assessment of future vulnerability of the global peatland carbon sink. *Nature Climate Change, 11*(1), 70-77. Retrieved from https://doi.org/10.1038/s41558-020-00944-0. doi:10.1038/s41558-020-00944-0

Loisel, J., Yu, Z., Beilman, D. W., Camill, P., Alm, J., Amesbury, M. J., et al. (2014). A database and synthesis of northern peatland soil properties and holocene carbon and nitrogen accumulation. *The Holocene, 24*(9), 1028-1042. Retrieved from https://doi.org/10.1177/0959683614538073. doi:10.1177/0959683614538073

López-Blanco, E., Jackowicz-Korczynski, M., Mastepanov, M., Skov, K., Westergaard-Nielsen, A., Williams, M., & Christensen, T. R. (2020). Multi-year data-model evaluation reveals the importance of nutrient availability over climate in arctic ecosystem c dynamics. *Environmental Research Letters, 15*(9), 094007. Retrieved from http://dx.doi.org/10.1088/1748-9326/ab865b. doi:10.1088/1748-9326/ab865b

López-Blanco, E., Lund, M., Williams, M., Tamstorf, M. P., Westergaard-Nielsen, A., Exbrayat, J. F., et al. (2017). Exchange of co2 in arctic tundra: Impacts of meteorological variations and biological disturbance. *Biogeosciences, 14*(19), 4467-4483. Retrieved from https://bg.copernicus.org/articles/14/4467/2017/. doi:10.5194/bg-14-4467-2017

MacDonald, G. M., Beilman, D. W., Kremenetski, K. V., Sheng, Y., Smith, L. C., & Velichko, A. A. (2006). Rapid early development of circumarctic peatlands and atmospheric ch₄ and co₂ variations. *Science, 314*(5797), 285. Retrieved from http://science.sciencemag.org/content/314/5797/285.abstract. doi:10.1126/science.1131722

McGuire, A. D., Lawrence, D. M., Koven, C., Clein, J. S., Burke, E., Chen, G., et al. (2018). Dependence of the evolution of carbon dynamics in the northern permafrost region on the trajectory of climate change. *Proceedings of the National Academy of Sciences, 115*(15), 3882. Retrieved from http://www.pnas.org/content/115/15/3882.abstract. doi:10.1073/pnas.1719903115

McGuire, A. D., Melillo, J. M., Joyce, L. A., Kicklighter, D. W., Grace, A. L., Moore Iii, B., & Vorosmarty, C. J. (1992). Interactions between carbon and nitrogen dynamics in estimating net primary productivity for potential vegetation in north america. *Global Biogeochemical Cycles, 6*(2), 101-124. Retrieved from https://doi.org/10.1029/92GB00219. doi:https://doi.org/10.1029/92GB00219

Meinshausen, M., Smith, S. J., Calvin, K., Daniel, J. S., Kainuma, M. L. T., Lamarque, J. F., et al. (2011). The rcp greenhouse gas concentrations and their extensions from 1765 to 2300. *Climatic Change, 109*(1), 213. Retrieved from https://doi.org/10.1007/s10584-011-0156-z. doi:10.1007/s10584-011-0156-z

Miao, C., Duan, Q., Sun, Q., Huang, Y., Kong, D., Yang, T., et al. (2014). Assessment of cmip5 climate models and projected temperature changes over northern eurasia. *Environmental Research Letters, 9*(5), 055007. Retrieved from http://dx.doi.org/10.1088/1748-9326/9/5/055007. doi:10.1088/1748-9326/9/5/055007

Minkkinen, K., Penttilä, T., & Laine, J. (2007). Tree stand volume as a scalar for methane fluxes in forestry-drained peatlands in finland. *Boreal Environment Research, 12*, 127-132.

Moore, T. R., Knorr, K.-H., Thompson, L., Roy, C., & Bubier, J. L. (2019). The effect of long-term fertilization on peat in an ombrotrophic bog. *Geoderma, 343*, 176-186. Retrieved from https://www.sciencedirect.com/science/article/pii/S0016706118322547. doi:https://doi.org/10.1016/j.geoderma.2019.02.034

Natali, S. M., Watts, J. D., Rogers, B. M., Potter, S., Ludwig, S. M., Selbmann, A.-K., et al. (2019). Large loss of co2 in winter observed across the northern permafrost region. *Nature Climate Change, 9*(11), 852-857. Retrieved from https://doi.org/10.1038/s41558-019-0592-8. doi:10.1038/s41558-019-0592-8

Nichols, J. E., & Peteet, D. M. (2019). Rapid expansion of northern peatlands and doubled estimate of carbon storage. *Nature Geoscience, 12*(11), 917-921. Retrieved from https://doi.org/10.1038/s41561-019-0454-z. doi:10.1038/s41561-019-0454-z

O'Donnell, J. A., Jorgenson, M. T., Harden, J. W., McGuire, A. D., Kanevskiy, M. Z., & Wickland, K. P. (2012). The effects of permafrost thaw on soil hydrologic, thermal, and carbon dynamics in an alaskan peatland. *Ecosystems, 15*(2), 213-229. Retrieved from https://doi.org/10.1007/s10021-011-9504-0. doi:10.1007/s10021-011-9504-0

Oberbauer, S. F., & Oechel, W. C. (1989). Maximum co_2-assimilation rates of vascular plants on an alaskan arctic tundra slope. *Holarctic Ecology, 12*(3), 312-316. Retrieved from http://www.jstor.org/stable/3682739.

Ojanen, P., Penttilä, T., Tolvanen, A., Hotanen, J.-P., Saarimaa, M., Nousiainen, H., & Minkkinen, K. (2019). Long-term effect of fertilization on the greenhouse gas exchange of low-productive peatland forests. *Forest Ecology and Management, 432*, 786-798. Retrieved from https://www.sciencedirect.com/science/article/pii/S0378112718311733. doi:https://doi.org/10.1016/j.foreco.2018.10.015

Palmer, M. D., Harris, G. R., & Gregory, J. M. (2018). Extending cmip5 projections of global mean temperature change and sea level rise due to thermal expansion using a physically-based emulator. *Environmental Research Letters, 13*(8), 084003. Retrieved from http://dx.doi.org/10.1088/1748-9326/aad2e4. doi:10.1088/1748-9326/aad2e4

Plaza, C., Pegoraro, E., Bracho, R., Celis, G., Crummer, K. G., Hutchings, J. A., et al. (2019). Direct observation of permafrost degradation and rapid soil carbon loss in tundra. *Nature Geoscience, 12*(8), 627-631. Retrieved from https://doi.org/10.1038/s41561-019-0387-6. doi:10.1038/s41561-019-0387-6

Qiu, C., Ciais, P., Zhu, D., Guenet, B., Peng, S., Petrescu, A. M. R., et al. (2021). Large historical carbon emissions from cultivated northern peatlands. *Science Advances, 7*(23), eabf1332. Retrieved from https://www.science.org/doi/abs/10.1126/sciadv.abf1332. doi:doi:10.1126/sciadv.abf1332

Raich, J. W., Rastetter, E. B., Melillo, J. M., Kicklighter, D. W., Steudler, P. A., Peterson, B. J., et al. (1991). Potential net primary productivity in south america: Application of a global model. *Ecol Appl, 1*(4), 399-429. doi:10.2307/1941899

Romanovsky, V. E., & Osterkamp, T. E. (1997). Thawing of the active layer on the coastal plain of the alaskan arctic. *Permafrost and Periglacial Processes, 8*(1), 1-22. Retrieved from https://doi.org/10.1002/(SICI)1099-1530(199701)8:1<1::AID-PPP243>3.0.CO;2-U. doi:https://doi.org/10.1002/(SICI)1099-1530(199701)8:1<1::AID-PPP243>3.0.CO;2-U

Schaefer, K., Zhang, T., Bruhwiler, L., & Barrett, A. (2011). Amount and timing of permafrost carbon release in response to climate warming. *Tellus B, 63*, 165-180. doi:10.1111/j.1600-0889.2011.00527.x

Sheffield, J., Barrett, A., Colle, B., Fernando, D., Fu, R., Geil, K., et al. (2013). North american climate in cmip5 experiments. Part i: Evaluation of historical simulations of continental and regional climatology*. *Journal of Climate, 26*, 9209-9245. doi:10.1175/JCLI-D-12-00592.1

Song, Y., Song, C., Ren, J., Tan, W., Jin, S., & Jiang, L. (2018). Influence of nitrogen additions on litter decomposition, nutrient dynamics, and enzymatic activity of two plant species in a peatland in northeast china. *Science of The Total Environment, 625*, 640-646. Retrieved from https://www.sciencedirect.com/science/article/pii/S0048969717337440. doi:https://doi.org/10.1016/j.scitotenv.2017.12.311

Sun, Z., Wang, Q., Batkhishig, O., & Ouyang, Z. (2016). Relationship between evapotranspiration and land surface temperature under energy- and water-limited conditions in dry and cold climates. *Advances in Meteorology, 2016*, 1835487. Retrieved from https://doi.org/10.1155/2016/1835487. doi:10.1155/2016/1835487

Treat, C. C., & Frolking, S. (2013). A permafrost carbon bomb? *Nature Climate Change, 3*(10), 865-867. Retrieved from https://doi.org/10.1038/nclimate2010. doi:10.1038/nclimate2010

Treat, C. C., & Jones, M. C. (2018). Near-surface permafrost aggradation in northern hemisphere peatlands shows regional and global trends during the past 6000 years. *The Holocene, 28*(6), 998-1010. Retrieved from https://doi.org/10.1177/0959683617752858. doi:10.1177/0959683617752858

Treat, C. C., Jones, M. C., Alder, J., Sannel, A. B. K., Camill, P., & Frolking, S. (2021). Predicted vulnerability of carbon in permafrost peatlands with future climate change and permafrost thaw in western canada. *Journal of Geophysical Research: Biogeosciences, n/a*(n/a), e2020JG005872. Retrieved from https://doi.org/10.1029/2020JG005872. doi:https://doi.org/10.1029/2020JG005872

Treat, C. C., Jones, M. C., Brosius, L., Grosse, G., Walter Anthony, K., & Frolking, S. (2021). The role of wetland expansion and successional processes in methane emissions from northern wetlands during the holocene. *Quaternary Science Reviews, 257*, 106864. Retrieved from https://www.sciencedirect.com/science/article/pii/S0277379121000718. doi:https://doi.org/10.1016/j.quascirev.2021.106864

Treat, C. C., Wollheim, W. M., Varner, R. K., Grandy, A. S., Talbot, J., & Frolking, S. (2014). Temperature and peat type control co2 and ch4 production in alaskan permafrost peats. *Global Change Biology, 20*(8), 2674-2686. Retrieved from https://doi.org/10.1111/gcb.12572. doi:https://doi.org/10.1111/gcb.12572

Turetsky, M. R., Donahue, W. F., & Benscoter, B. W. (2011). Experimental drying intensifies burning and carbon losses in a northern peatland. *Nature Communications, 2*(1), 514. Retrieved from https://doi.org/10.1038/ncomms1523. doi:10.1038/ncomms1523

Turetsky, M. R., Wieder, R. K., & Vitt, D. H. (2002). Boreal peatland c fluxes under varying permafrost regimes. *Soil Biology and Biochemistry, 34*(7), 907-912. Retrieved from http://www.sciencedirect.com/science/article/pii/S0038071702000226. doi:https://doi.org/10.1016/S0038-0717(02)00022-6

Turunen, J., Roulet, N. T., Moore, T. R., & Richard, P. J. H. (2004). Nitrogen deposition and increased carbon accumulation in ombrotrophic peatlands in eastern canada. *Global Biogeochemical*

Cycles, 18(3). Retrieved from https://doi.org/10.1029/2003GB002154. doi:https://doi.org/10.1029/2003GB002154

Turunen, J., Tomppo, E., Tolonen, K., & Reinikainen, A. (2002). Estimating carbon accumulation rates of undrained mires in finland–application to boreal and subarctic regions. *The Holocene, 12*(1), 69-80. Retrieved from https://doi.org/10.1191/0959683602hl522rp. doi:10.1191/0959683602hl522rp

Updegraff, K., Bridgham, S. D., Pastor, J., Weishampel, P., & Harth, C. (2001). Response of co₂ and ch₄ emissions from peatlands to warming and water table manipulation. *Ecological Applications, 11*(2), 311-326. Retrieved from http://www.jstor.org/stable/3060891. doi:10.2307/3060891

Wang, C., Wan, S., Xing, X., Zhang, L., & Han, X. (2006). Temperature and soil moisture interactively affected soil net n mineralization in temperate grassland in northern china. *Soil Biology and Biochemistry, 38*(5), 1101-1110. Retrieved from https://www.sciencedirect.com/science/article/pii/S0038071705003251. doi:https://doi.org/10.1016/j.soilbio.2005.09.009

Wang, S., Zhuang, Q., & Yu, Z. (2016). Quantifying soil carbon accumulation in alaskan terrestrial ecosystems during the last 15 000 years. *Biogeosciences, 13*(22), 6305-6319. Retrieved from https://bg.copernicus.org/articles/13/6305/2016/. doi:10.5194/bg-13-6305-2016

Wang, S., Zhuang, Q., Yu, Z., Bridgham, S., & Keller, J. K. (2016). Quantifying peat carbon accumulation in alaska using a process-based biogeochemistry model. *Journal of Geophysical Research: Biogeosciences, 121*(8), 2172-2185. Retrieved from https://doi.org/10.1002/2016JG003452. doi:https://doi.org/10.1002/2016JG003452

Weiss, R., Shurpali, N., Sallantaus, T., Laiho, R., Laine, J., & Alm, J. (2006). Simulation of water table level and peat temperatures in boreal peatlands. *ECOLOGICAL MODELLING, 192*, 441-456. doi:10.1016/j.ecolmodel.2005.07.016

Williams, T. G., & Flanagan, L. B. (1996). Effect of changes in water content on photosynthesis, transpiration and discrimination against 13co2 and c18o16o in pleurozium and sphagnum. *Oecologia, 108*(1), 38-46. Retrieved from https://doi.org/10.1007/BF00333212. doi:10.1007/BF00333212

Yu, Z., Beilman, D., & Jones, M. (2009). Sensitivity of northern peatland carbon dynamics to holocene climate change. *Washington DC American Geophysical Union Geophysical Monograph Series, 184*, 55-69. doi:10.1029/2008GM000822

Yu, Z., Vitt, D. H., & Wieder, R. K. (2014). Continental fens in western canada as effective carbon sinks during the holocene. *The Holocene, 24*(9), 1090-1104. Retrieved from https://doi.org/10.1177/0959683614538075. doi:10.1177/0959683614538075

Zhu, F., Emile-Geay, J., McKay, N., Hakim, G., Khider, D., Ault, T., et al. (2019). Climate models can correctly simulate the continuum of global-average temperature variability. *Proceedings of the National Academy of Sciences*. doi:10.1073/pnas.1809959116

Zhuang, Q., McGuire, A. D., O'Neill, K. P., Harden, J. W., Romanovsky, V. E., & Yarie, J. (2002). Modeling soil thermal and carbon dynamics of a fire chronosequence in interior alaska. *Journal of Geophysical Research: Atmospheres, 107*(D1), FFR 3-1-FFR 3-26. Retrieved from https://doi.org/10.1029/2001JD001244. doi:https://doi.org/10.1029/2001JD001244

Zhuang, Q., Melillo, J. M., Kicklighter, D. W., Prinn, R. G., McGuire, A. D., Steudler, P. A., et al. (2004). Methane fluxes between terrestrial ecosystems and the atmosphere at northern high latitudes during the past century: A retrospective analysis with a process-based biogeochemistry model. *Global Biogeochemical Cycles, 18*(3). Retrieved from https://doi.org/10.1029/2004GB002239. doi:https://doi.org/10.1029/2004GB002239

Zhuang, Q., Romanovsky, V., & McGuire, A. (2001). Incorporation of a permafrost model into a large-scale ecosystem model: Evaluation of temporal and spatial scaling issues in simulating soil thermal dynamics. *Journal of Geophysical Research, 106*, 33649-33670. doi:10.1029/2001JD900151